Available online at www.sciencedirect.com

SciVerse ScienceDirect

Geochimica et Cosmochimica Acta 112 (2013) 226–250

Geochimica et Cosmochimica Acta

www.elsevier.com/locate/gca

Vapor saturation of sodium: Key to unlocking the origin of chondrules

Alexei V. Fedkin *, Lawrence Grossman [1]

Dept. of the Geophysical Sciences, The University of Chicago, 5734 South Ellis Ave., Chicago, IL 60637, United States

Received 16 October 2012; accepted in revised form 14 February 2013; available online 26 February 2013

Abstract

Sodium saturation of the vapor coexisting with chondrules at their liquidus temperatures implies that vapor-condensed phase equilibrium was reached at those temperatures for all elements more refractory than sodium. In order to investigate the possibility that chondrules formed in impact-generated plumes, equilibrium calculations were applied to droplets made from two different target compositions. Combinations of dust enrichment and P^{tot} were found that lead to sodium saturation, and the subsequent chemical and mineralogical evolution of the droplets was explored at those conditions. If an impact on a body of CI composition caused instantaneous heating, melting and devolatilization of the target rock and ejection of a plume of gaseous, liquid and solid matter that mixed with residual nebular gas at conditions where 50% or 90% of the sodium was retained by the resulting droplets at their liquidus temperature, their mineralogical and chemical properties would strongly resemble those of Type II chondrules. If the droplets cooled and equilibrated with the mixture of residual nebular gas and their devolatilized water, sulfur and alkalis, the fayalite content of the olivine and the chemical compositions of the bulk droplets and their glasses would closely resemble those of Types IIA and IIAB chondrules at CI dust enrichments between 400× and 800×. For 50% sodium retention, the corresponding values of P^{tot} are 2 bars (for 400×) and 1 bar (for 800×). For 90% retention, they are 25 and 10 bars, respectively. If, instead, the target has an anhydrous, ordinary chondrite-like composition, called H′, the ejected droplets are bathed in a gas mix consisting mostly of devolatilized sulfur and alkalis with residual nebular gas, a much more reducing plume. If the conditions were such that sodium were retained by the resulting droplets at their liquidus temperature, the fayalite contents of the olivine and the chemical compositions of the bulk droplets and their glasses would closely resemble those of Types IA and IAB chondrules at H′ dust enrichments between $10^3\times$ and $4\times10^3\times$. For 90% sodium retention, the corresponding values of P^{tot} are 15 bars (for $10^3\times$) and 2 bars (for $4\times10^3\times$). For 50% retention, they are 2 and 8×10^{-2} bars, respectively.

1. INTRODUCTION

Chondrules are silicate-rich, glassy spherules that existed as independent liquid droplets somewhere in the solar nebula. The textures of porphyritic chondrules can be reproduced in the laboratory by heating solid precursors to temperatures where abundant crystal nuclei survive, either just below the liquidus, or above the liquidus for too short a time to destroy all pre-existing nuclei (Hewins and Radomsky, 1990). Barred chondrules are produced from melts in which solid precursors are heated above the liquidus, and almost all pre-existing nuclei are destroyed (Hewins and Radomsky, 1990). Although a continuum of compositions may exist, Types I and II chondrules are defined as having mean Fe/(Fe + Mg) cation ratios <0.1 and $\geqslant0.1$, respectively, in their olivine and pyroxene. The two types differ in their total iron contents, with the mean CI-normalized Fe/Si ratios of Type Is being ~0.07 (Jones and Scott, 1989; Jones, 1994) and those of Type IIs ~0.33 (Jones, 1990, 1996). They also differ in their alkali contents, with mean CI-normalized Na/Si and K/Si atomic ratios of 0.35 and 0.41 in Type Is and 1.09 and 1.24 in Type IIs.

* Corresponding author.
E-mail address: avf@uchicago.edu (A.V. Fedkin).
[1] Enrico Fermi Institute, The University of Chicago, United States.

0016-7037/$ - see front matter © 2013 Elsevier Ltd. All rights reserved.
http://dx.doi.org/10.1016/j.gca.2013.02.020

The iron and alkali abundances are illustrative of a more general depletion in elements more volatile than Si in Type I and, to a lesser extent, Type II chondrules compared to CI chondrites (Jones et al., 2005). Such depletions are expected to result from evaporation when chondrule precursors are heated to near-liquidus temperatures in hydrogen-rich cosmic gases, a process that would also produce heavy isotope enrichments in the fractions of the evaporated elements that remain in chondrules (Davis et al., 2005). Because large isotopic mass-fractionations of moderately volatile elements are not observed in bulk compositions of chondrules (Davis et al., 2005), evaporation either did not occur or was followed by recondensation, although Richter et al. (2011) demonstrated evaporation conditions for suppression, but not elimination, of large isotopic fractionations. To suppress evaporation and/or promote recondensation, models have been proposed in which chondrule formation occurred in regions highly enriched in dust relative to gas compared to solar composition (Alexander et al., 2008) or at high total pressure (Fedkin et al., 2012).

Alexander et al. (2008) found Na in the cores of olivine crystals in both barred and porphyritic chondrules of Types I and II, and showed that no more than 10% of the Na was lost from chondrules while they crystallized. From Na analyses in olivine phenocrysts, glass inclusions and mesostases in Type II chondrules in Semarkona, Hewins et al. (2012) found evidence that the bulk Na concentration first declined and then increased during olivine crystallization but that Na loss was limited to ~50%.

Fedkin et al. (2012) used a kinetic evaporation model to show, for thermal histories with fast heating, near-liquidus peak temperatures and cooling rates like those of natural chondrules, that huge Fe and alkali losses occur at a total pressure of 4×10^{-4} bar, even when dust is enriched 600 times relative to solar composition. The model shows further that, although these elements eventually recondense during cooling, resulting in near-normal isotopic composition for bulk chondrules, recondensation occurs only after large amounts of olivine crystallize that preserve very large, evaporation-induced Fe isotopic mass-fractionations that existed in the liquid before much of the Fe recondensed. Because Fe isotopic variations of the predicted size had not been found within individual chondrules, Fedkin et al. (2012) concluded that very little Fe evaporated at any stage of chondrule formation. For the same thermal history, they showed that increasing the dust enrichment to $6 \times 10^4\times$ at 4×10^{-4} bar, or the total pressure to 4×10^{-2} bar at a dust enrichment of 600×, dramatically reduces the fraction of the Fe evaporated, the range of the internal δ^{56}Fe variations and the fraction of the olivine in a chondrule that exhibits any isotopic fractionation. Even at these extreme conditions, however, more than 90% of the Na and K still evaporate. Regardless of whether 10% or 50% of the Na evaporated from chondrules, the dust enrichments (Alexander and Ebel, 2012; Fedkin et al., 2012) and total pressures (Fedkin et al., 2012) required for the corresponding degrees of Na retention are so much higher than these values that Fedkin et al. (2012) suggested that chondrules more likely formed in impact-generated plumes than in the initial cooling and contraction stage of the nebular disk.

In the first part of this paper, the kinetic evaporation model of Fedkin et al. (2012) is used to show why limited Na loss requires such extreme conditions and why it implies establishment of gas-condensed phase equilibrium. In the second part of the paper, equilibrium calculations are used to predict the mineralogical and chemical compositions of droplets formed under conditions that satisfy the Na retention constraints, to compare them to those of natural chondrules, to constrain the compositions of precursor solids, and to explore the ramifications of the extreme dust enrichments and/or total pressures for the origin of chondrules.

2. SODIUM RETENTION CONDITIONS

2.1. Vapor pressure of sodium over model chondrule compositions

Construction of model chondrule compositions started with the relative atomic abundances of Si, Ti, Al, Cr, Fe, Ni, Mn, Mg, Ca, Na and K from Anders and Grevesse (1989). To account for depletions of moderately volatile elements, 93% of the Fe, 95% of the Ni and 70% of the Na and K were removed for the model Type I chondrule, and 33% of the Fe and Ni for the model Type II. Using the MELTS model of Ghiorso and Sack (1995), the equilibrium assemblage for the resulting Type I cation proportions was calculated at two different oxygen fugacities, corresponding to log f_{O_2} of IW-3 (i.e., 3 log units below the iron-wüstite buffer) and IW-1, and for the Type II proportions at IW-2 and IW-1, each at its respective liquidus temperature. The resulting ranges in the ratio of FeO to metallic Fe, shown in Table 1, span the ranges seen in natural Types I (Jones and Scott, 1989; Jones, 1994) and II (Jones, 1990, 1996) chondrules.

Table 1
Model chondrule compositions (wt.%).

log fO_2	Type I		Type II	
	IW-3	IW-1	IW-2	IW-1
Liquidus	1960 K	1957 K	1952 K	1935 K
SiO_2	51.11	50.78	44.45	43.75
TiO_2	0.16	0.16	0.14	0.14
Al_2O_3	3.68	3.66	3.20	3.15
Cr_2O_3	0.87	0.87	0.76	0.75
FeO	1.10	3.83	8.19	15.04
MnO	0.58	0.57	0.50	0.49
MgO	36.82	36.59	32.03	31.52
NiO	0.00	0.16	0.00	0.08
CaO	2.91	2.90	2.53	2.49
Na_2O	0.45	0.45	1.32	1.30
K_2O	0.05	0.05	0.13	0.13
Fe	2.14	0.00	6.03	0.51
Ni	0.12	0.00	0.71	0.64
Atomic Fe/Si rel. to CI		0.07		0.33
Atomic Na/Si rel. to CI		0.30		1.00
Atomic K/Si rel. to CI		0.30		1.00

The evaporation reaction of Na from a ferromagnesian liquid can be written as

$$Na_2SiO_{3(l)} \Longleftrightarrow 2Na_{(g)} + SiO_{2(l)} + 1/2O_{2(g)}, \quad (1)$$

from which,

$$P^v_{Na} = \sqrt{K_1 a_{Na_2SiO_3}/a_{SiO_2} f^{1/2}_{O_2}}, \quad (2)$$

where P^v_{Na} is the equilibrium vapor pressure of monatomic Na, K_1 is the equilibrium constant for reaction (1) and $a_{Na_2SiO_3}$ and a_{SiO_2} are the activities of Na_2SiO_3 and SiO_2 in the liquid, respectively. The equilibrium vapor pressure of Na is seen to be a function of the equilibrium f_{O_2} of the assemblage. Using MELTS to calculate the activities and the same thermodynamic data as in Fedkin et al. (2012) to calculate K_1, P^v_{Na} was computed for the Type I and Type II model chondrule compositions, each as a function of temperature at two different, fixed values of f_{O_2}. Results are shown in Fig. 1a and b for the model Type I and model Type II chondrule compositions, respectively. At fixed f_{O_2}, P^v_{Na} falls by ~1 order of magnitude as the temperature falls from the liquidus to 200 K lower. At constant temperature, P^v_{Na} falls by ~50% when f_{O_2} increases by 1 log unit. At constant temperature and f_{O_2}, the lower Na content of the Type I composition compared to the Type II results in a lower P^v_{Na} by a factor of ~3. In general, the equilibrium vapor pressure of Na over Type I and Type II chondrule compositions is on the order of 10^{-3}–10^{-4} bar for the 200 K temperature interval immediately below their liquidi.

2.2. Evaporation of sodium in a closed system

Evaporation rates are governed by the Hertz-Knudsen equation, written here for the case of monatomic sodium evaporating in a closed system consisting of a droplet and its ambient gas that are in thermal equilibrium with one another,

$$J_{Na} = \frac{\gamma^e_{Na} P^v_{Na}}{\sqrt{2\pi M_{Na} RT}} - \frac{\gamma^c_{Na} P^a_{Na}}{\sqrt{2\pi M_{Na} RT}}. \quad (3)$$

In Eq. (3), J_{Na} is the flux of sodium across the droplet-gas interface in moles cm^{-2} s^{-1}, R is the gas constant, M_{Na}, γ^e_{Na}, γ^c_{Na}, and P^v_{Na} are the atomic weight, evaporation coefficient, condensation coefficient, and equilibrium vapor pressure of Na, respectively, and P^a_{Na} is the partial pressure of monatomic Na in the ambient gas. The first term on the right-hand side is the evaporation rate and the second term is the condensation rate. Evaporation coefficients are measured in kinetic experiments. Condensation coefficients are more poorly known, and are generally assumed to be equal to evaporation coefficients. For the case of $\gamma^e_{Na} = \gamma^c_{Na}$, it is seen that, when $P^v_{Na} > P^a_{Na}$, J_{Na} is positive and net evaporation occurs but when $P^v_{Na} < P^a_{Na}$, J_{Na} is negative and net condensation occurs. For the special case of $P^v_{Na} = P^a_{Na}$, the evaporation rate is equal to the condensation rate, $J_{Na} = 0$ and the system is at equilibrium.

Alexander et al. (2008) concluded that evaporation of Na from chondrules stopped after no more than 10% of their initial Na was lost. Included among the samples of that study were many porphyritic chondrules of Types I and II, in which there was measurable Na in the cores of olivine phenocrysts. Because a condition for forming porphyritic chondrules is that almost all pre-existing solid nuclei were destroyed, the peak temperatures reached by porphyritic chondrules must have been very close to the liquidus, and the very first olivine to crystallize, that in phenocryst cores, did so immediately upon cooling from that temperature. The fact that retention of at least 90% of the Na by the coexisting liquid is recorded by the phenocryst cores means that the condition that the ambient pressure of Na equaled its equilibrium vapor pressure was achieved at the liquidus. Sodium retention was also demonstrated for barred chondrules by Alexander et al. (2008), but olivine incoming temperatures are poorly known for those objects because of subcooling. Consequently, the focus of the present paper is on porphyritic chondrules. As seen in Section 2.1, the vapor pressure of Na at the liquidus temperatures of Types I and II chondrules is $\sim 10^{-3}$ bar, which is much higher than the partial pressure of Na in a gas of solar composition at canonical nebular pressures. Because the atomic Na/H ratio in solar gas is $\sim 10^{-6}$, the partial pressure of Na in solar gas is only $\sim 10^{-12}$–10^{-9} bar when the total hydrogen pressure is 10^{-6}–10^{-3} bar. Achieving an ambient pressure of Na of $\sim 10^{-3}$ bar would require either enhancement of the total pressure by a factor $\geqslant 10^6$ relative to canonical nebular pressures or enhancement of the abundance of Na relative to H via dust enrichment of $\geqslant 10^6$ relative to solar abundances.

2.3. Evaporation calculations

The closed-system, kinetic evaporation model of Fedkin et al. (2012) was used to determine the conditions necessary for retention of both 50% and 90% of the Na in each of the model chondrule compositions shown in Table 1. This model tracks mineralogical, chemical and isotopic changes that would occur in clumps of solid chondrule precursors subjected to various input pressure–temperature histories while immersed in an ambient gas. Evaporation and condensation rates are computed for each element from equations analogous to Eq. (3) using evaporation coefficients obtained from volatilization experiments (Hashimoto, 1983; Wang et al., 2001; Richter et al., 2009; Tachibana et al., 2011). In the present case, the dust was assumed to be heated instantaneously to its liquidus temperature, where it formed a droplet of 0.5 mm radius, and to begin cooling immediately at 10 or 100 K/h. The droplet and gas were assumed to be in thermal equilibrium throughout the calculation. Initially, all of the H, He, C, N, P and S in the system was assumed to be in the gas and all of the Ca, Al, Ti, Si, Mg, Fe, Ni, Cr, Mn, Na and K was assumed to be in the droplet. The oxygen abundance in the droplet was dictated by the equilibrium f_{O_2} of the model chondrule. Before dust enrichment, the relative atomic abundances in the total system were assumed to be solar, except for those of Fe and Ni, which are depleted relative to Si because of their depletions in both the model Type I and Type II chondrule compositions, and Na and K, which are depleted only in the model Type I composition, as in measurements of natural samples. A trial-and-error method was used to find

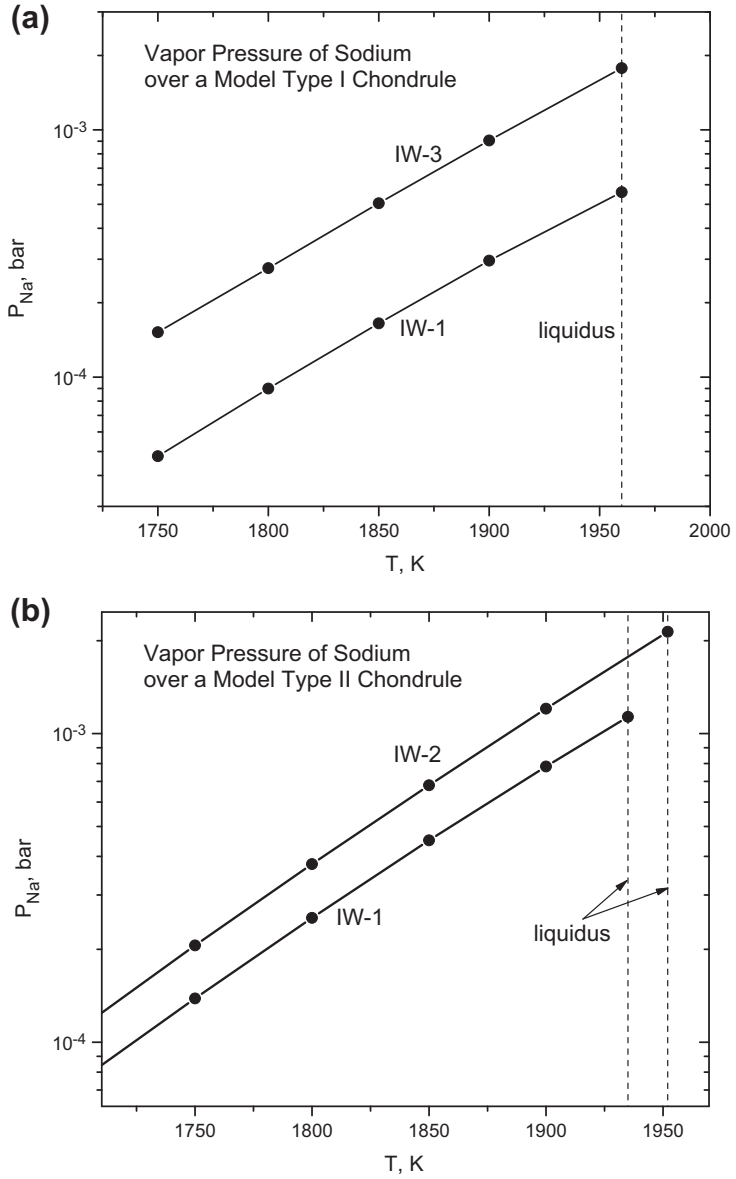

Fig. 1. Equilibrium vapor pressure of sodium calculated as a function of temperature at the liquidus and below for (a) the model Type I and (b) the model Type II chondrule composition at each of their respective oxygen fugacities shown in Table 1.

combinations of dust enrichment and total pressure at which P^{a}_{Na} became just equal to P^{v}_{Na} after only 10% or only 50% Na loss from the droplet. In these cases, dust enrichment is defined as enrichment in dust of the compositions listed in Table 1. The total pressure variable employed is P^{tot}_{H}, which is the sum of the partial pressures of all hydrogen species, each multiplied by its number of hydrogen atoms per molecule.

An example of a successful calculation is shown in Fig. 2 for the case of a Type I model chondrule with an equilibrium log f_{O_2} of IW-3 at its 1960 K liquidus temperature, immersed in gas with P^{tot}_{H} of 10^{-4} bar at a dust enrichment of 2.8×10^{8}, and cooled at 100 K/h. As the fraction of Na evaporated increases with time, the vapor pressure of Na falls very slightly in response to the declining Na_2O content of the droplet. The partial pressure of Na in the ambient gas rises, very sharply at first and then more gently, until the two pressures become equal when exactly 10% of the Na has been lost. At this point, the Na_2O content of the droplet is in equilibrium with the gas and net evaporation stops. As this degree of Na loss occurs in only ~0.5 s in this case, the particular combination of dust enrichment and P^{tot}_{H} needed to achieve this saturation condition is unaffected by whether the cooling rate is 10 or 100 K/h. At both cooling rates, 10% Na loss occurs virtually isothermally.

The fast evaporation rate of Na at these temperatures raises the question of whether the diffusion rate of Na is fast enough to support the evaporation rate. Richter et al. (2011) measured a K diffusion coefficient, D_K, $>2 \times 10^{-4}$ cm^2 s^{-1} in a chondrule-like melt at 1923 K. Sodium diffuses faster than K, as seen in data reviewed by Zhang et al. (2010), from which $D_{Na}/D_K \sim 30$ for rhyolite melt at

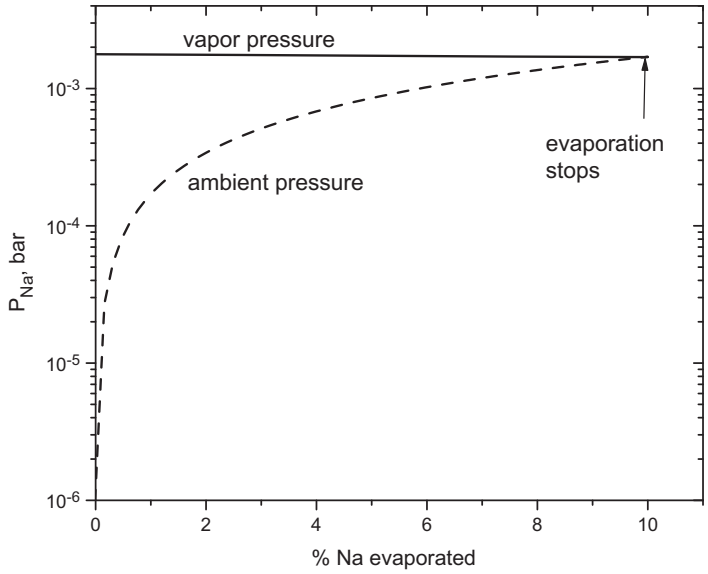

Fig. 2. Evolution of the equilibrium vapor pressure and ambient pressure of sodium during closed-system evaporation from the model Type I chondrule whose log f_{O_2} is IW-3 at its liquidus temperature of 1960 K. When P_H^{tot} in the ambient, complementary solar gas is 10^{-4} bar, the system is enriched in chondrules of this composition by a factor of 2.8×10^8 relative to solar composition and cooling occurs at 100 K/h starting at the liquidus, the ambient pressure and vapor pressure become equal after exactly 10% sodium loss, which occurs in <1 s. When this condition is met, the Na_2O content of the droplet is in equilibrium with the gas, and evaporation stops.

1200 K. Combining these data yields $D_{Na} > 0.006\ cm^2\ s^{-1}$ for a near-liquidus, chondrule-like liquid. The diffusion time of Na from the center to the edge of a 0.5 mm-radius molten chondrule near its liquidus is only $\sim(0.05\ cm)^2/6 \times 10^{-3}\ cm^2\ s^{-1} = 0.4$ s. Thus, the diffusion time is shorter than the evaporation time.

The conditions discovered by this approach are shown in Fig. 3a and b for the Type I and Type II model chondrule compositions, respectively. For both chondrule types, the dust enrichment needed to stop Na loss at the liquidus falls from $\sim 10^{10}$ at $P_H^{tot} = 10^{-6}$ bar to $\sim 10^2$ at $P_H^{tot} = 10^2$ bar regardless of which equilibrium f_{O_2} is used or whether 10% or 50% of the Na is allowed to evaporate before reaching that condition. For fixed P_H^{tot} and percent Na loss, the needed dust enrichment falls by a factor of ~2 per 1 log unit increase in f_{O_2}. For fixed P_H^{tot} and f_{O_2}, the needed dust enrichment falls by a factor of ~6 when the Na loss rises from 10% to 50%. The pronounced inverse relationship between the needed dust enrichment and P_H^{tot} is merely a consequence of the facts that $P_{Na}^a \sim P_{Na}^{tot}$ and

$$P_{Na}^{tot} = \frac{A(Na)P_H^{tot}}{A(H)}, \quad (4)$$

where A(Na) and A(H) are the atomic abundances of sodium and hydrogen in the gas, respectively. Thus, to maintain a constant value of P_{Na}^a for a given percent of Na evaporation while decreasing P_H^{tot} by some factor requires only that Na-containing, H-free dust be enriched relative to gaseous hydrogen by the same factor.

2.4. Environment for chondrule formation

In the lower left of both Fig. 3a and b is a rectangular region labeled "solar nebula", drawn over a range of P_H^{tot} from 10^{-3} to 10^{-6} bar and from no dust enrichment to a maximum of 125×. The pressure range, taken from the work of Ruden and Pollack (1991) and referred to herein as the canonical range of nebular pressures, is characteristic of midplane regions from 0.6 to 4 AU from the center of the solar nebula over the first 3×10^4 years of its history. The upper bound on the dust enrichment for the solar nebula is the maximum value found in Cassen's (2001) gravitational settling model. Although Cuzzi et al. (2001) found that much higher dust enrichments are possible in turbulent concentration models, the probability of achieving dust enrichments $\gg 10^2$ drops off dramatically with increasing dust enrichment, making this mechanism unsuitable for explaining the great abundance of chondrules.

Inspection of Fig. 3a and b shows that the required combinations of dust enrichment and P_H^{tot} lie very far from the canonical range of solar nebular conditions, regardless of the composition of the chondrule or its equilibrium oxygen fugacity, or whether 10% or 50% Na loss occurs before the vapor becomes saturated. Over the canonical range of nebular pressures, the needed dust enrichments range from 10^6 to 10^{11}, 10^4 to 10^9 times higher than the maximum dust enrichment attained in gravitational settling models. Alternatively, at the maximum dust enrichment achievable in gravitational settling models, the condition for Na retention is at $P_H^{tot} > 1$ bar, more than 10^3 times higher than the upper end of the canonical range of nebular pressures.

Grossman et al. (2012) showed that stabilization of the FeO contents of high-temperature liquids with compositions like those of both Type I and Type II chondrules requires oxygen fugacities at least 5 log units higher than that of a solar gas. They also showed that such conditions could be achieved in a gas whose composition is solar except for enrichment in water by a factor of at least several

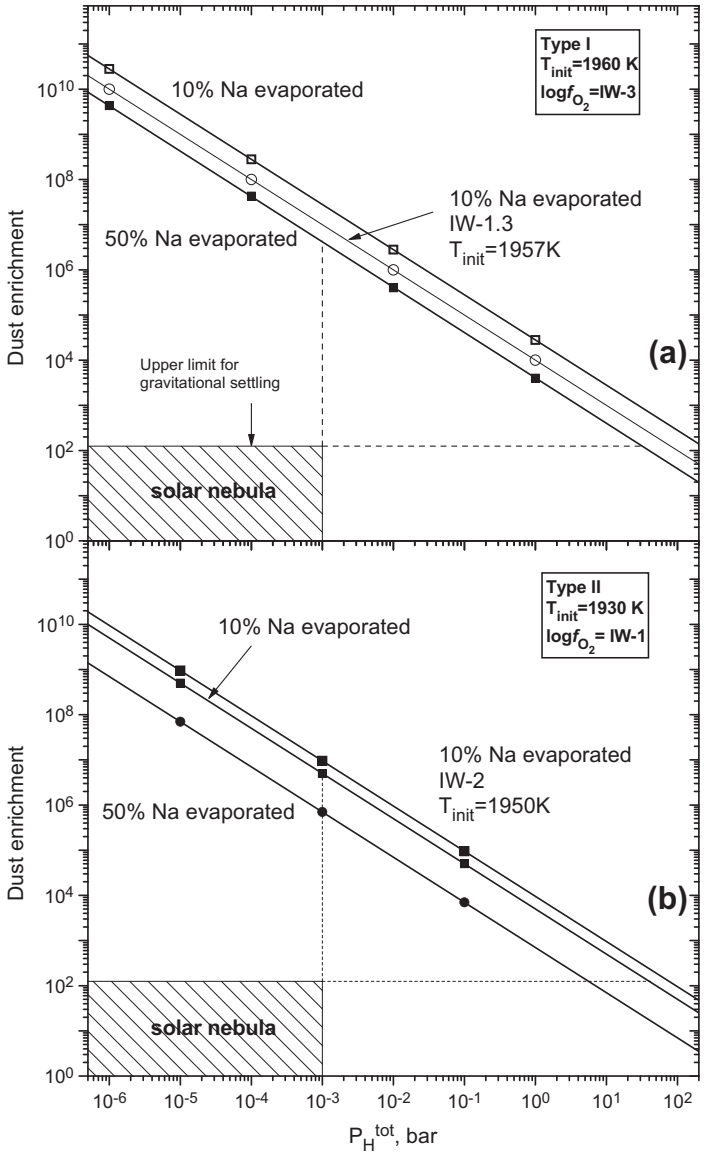

Fig. 3. Combinations of chondrule enrichment and P_H^{tot} of the ambient gas that cause sodium evaporation to stop after 10% or 50% sodium loss when (a) model Type I and (b) model Type II chondrules of the indicated equilibrium oxygen fugacities are cooled at 100 K/h from their respective liquidus temperatures. The regions labeled "solar nebula" span the canonical range of nebular total pressures from dynamical models of the solar nebula and extend to the maximum dust enrichment in gravitational settling models.

hundred. The most effective way of enriching a nebular region in water, however, transport of icy planetesimals from the outer part of the nebula to the inner part, is unable to produce water enrichments greater than a factor of 10 (Ciesla and Cuzzi, 2006). For this and other reasons, Grossman et al. (2012) concluded that it is unlikely that appreciable oxidized iron existed in the inner solar system at the end of the primary cooling and condensation stage of the solar nebula. They suggested instead that the first generation of planetesimals accreted from reduced nebular condensates and water ice, that the first FeO formed inside such parent bodies when liquid water interacted with metallic nickel–iron and magnesium silicates at elevated temperature, and that the resulting assemblage was the source of chondrule precursors. The huge differences between the f_{O_2}, P_H^{tot} and dust enrichment required by chondrule chemical properties and the values of those parameters achievable during the contraction stage of the solar nebular disk suggest that a more likely regime for chondrule formation is in liquid + -solid + vapor plumes generated by impacts on FeO-containing planetesimals (Fedkin et al., 2012; Grossman et al., 2012).

3. PHASE EQUILIBRIUM COMPUTATION OF CHONDRULE PHASE ASSEMBLAGES

3.1. Computational method

When a chondrule-like liquid undergoes closed-system evaporation while cooling at 10 or 100 K/h through near-

liquidus temperatures, elements that are less volatile than Na, such as K, Fe, Mg and Si, reach saturation in the vapor within seconds of the time when Na stops evaporating and, with the exception of K, after much smaller fractional evaporation losses than Na (Fedkin et al., 2012). This means that, under the conditions explored here, when Na evaporation stops after 10% or 50% loss at the chondrule liquidus temperature, all of the less volatile elements will have also reached saturation before significant cooling occurs, and the entire chondrule will be at vapor-condensed phase equilibrium.

In Section 2, conditions for Na retention were investigated in systems of assumed P_H^{tot} that had become enriched in dust of specific chondrule compositions. In the present section, the impact hypothesis is tested by modeling systems formed by mixing ejecta from parent bodies of specific compositions with their respective complementary gas compositions. In anticipation that Types I and II chondrules might require different starting materials from one another, two parent body compositions with contrasting oxygen abundances were assumed, and their compositions are listed in Table 2. The CI chondrite composition (Anders and Grevesse, 1989) is an obvious choice for the Type IIs because the latter have nearly solar mean alkali/Si ratios and because the mineralogical composition of CIs is similar to that expected to result from interaction of liquid water with nebular condensates. A more reduced starting material was selected for the Type Is, derived from the mean composition of H chondrite falls (Jarosewich, 1990). Type I chondrules are depleted in alkalis relative to Si by ~70% compared to CIs but acted as closed systems with respect to Na during crystallization, so the depletion must be characteristic of the parent. Because alkalis are depleted relative to Si by only ~20% in H chondrites compared to CIs, the parent composition used for Type Is in the present work, called H′, was derived from the mean H chondrite fall composition of Jarosewich (1990) by removal of sufficient K and Na to yield alkali/Si ratios that are 30% of those in CI chondrites.

Table 2
Bulk chemical compositions of starting materials (atoms/10^6 Si).

	CI (Anders and Grevesse, 1989)	H′* (after Jarosewich, 1990)
O	7.63E+06	3.42E+06
H	5.28E+06	5.84E+04
Mg	1.07E+06	9.47E+05
Si	1.00E+06	1.00E+06
Fe	9.00E+05	8.06E+05
C	7.56E+05	1.50E+04
S	4.46E+05**	1.01E+05
Al	8.49E+04	6.89E+04
Ca	6.11E+04	5.09E+04
N	5.98E+04	0.00E+00
Na	5.74E+04	1.72E+04
Ni	4.93E+04	3.82E+04
Cr	1.35E+04	1.12E+04
P	1.04E+04	6.25E+03
Mn	9.55E+03	7.17E+03
K	3.77E+03	1.13E+03
Ti	2.40E+03	2.47E+03
Co	2.25E+03	2.23E+03
Atomic Na/Si	5.74E−02	1.72E−02
Atomic K/Si	3.77E−03	1.13E−03

* H′ is average H chondrite with Na/Si and K/Si = 0.3× CI.
** From Lodders (2003).

It was shown above that Na saturation at chondrule liquidus temperatures implies that chondrules were in gas-condensed phase equilibrium. Therefore, in the present work, an equilibrium calculation is used to predict phase assemblages at specific combinations of dust enrichment and P^{tot} where 50% or 90% of the Na is condensed at the peak temperature of olivine stability. The objective is to compare the mineralogical and chemical properties of the predicted assemblages with those of natural chondrules. The computer program employed herein is VAPORS, a code constructed from the MELTS program of Ghiorso and Sack (1995) and used by Ebel and Grossman (2000) for condensation calculations. A condensation calculation is merely a series of independent equilibrium calculations carried out at successively lower temperatures. The VAPORS code is capable of computing multicomponent, multiphase equilibrium assemblages even after much of the vapor has condensed. This is an important consideration in the present work, because, except for S and alkalis, all of the major condensable elements are virtually totally condensed when only 10% or 50% of the Na is gaseous. Thus, the following computational results should not be considered a description of chondrule condensation. The relevant part of the calculation begins after the chondrule parent material is heated to the liquidus, where only a fraction of the Na is in the gas, and describes changes in the equilibrium phase assemblage due to crystallization of the liquid and redox processes as the remainder of the alkalis and S condense while the temperature falls. Each such calculation requires ~6 h on an iMac computer equipped with a 2.8 GHz Intel Core i7 processor. A trial-and-error method was used to select combinations of dust enrichment and P^{tot} at which to run the VAPORS code in search of those where the desired degree of sodium retention occurs at the maximum temperature of olivine stability.

Formation of ortho- and clinopyroxene was suppressed in most runs to simulate formation conditions of porphyritic olivine (PO) chondrules, in which pyroxene failed to nucleate due to rapid cooling. When a comparison of compositions of model liquids to those of glasses in pyroxene-bearing chondrules was desired, runs were performed in which pyroxenes were allowed to form. Because pyroxene always becomes stable at temperatures well below the incoming temperature of olivine, where all components of the silicate portion of the droplet are nearly totally condensed, the presence or absence of pyroxene affects neither the equilibrium conditions necessary for sodium retention nor the bulk composition of the droplet. Whenever near-total condensation occurs, however, use of the VAPORS code becomes limited because differences arise in chemical potentials of components between gas and condensed phases, a sign of poor convergence (Ebel and Grossman, 2000).

Therefore, whenever it was desirable to trace the chemical evolution of relatively low-temperature liquids ($T < 1300$–1500 K), exploration of liquid–crystal phase relations was done using the MELTS program. The MELTS calculations were initiated with the f_{O_2} and silicate bulk composition computed at the lowest-temperature step of the VAPORS program at which a difference for any condensed component was still $<10^{-5}$ of the chemical potential in the gas. This step is equivalent to assuming that the silicate fraction of the system acted as a closed system over the temperature interval of interest.

3.2. Mixtures of residual nebular gas with heated CI chondrite

3.2.1. Conditions for sodium retention at the maximum temperature of olivine stability

Results for CI dust are shown in Fig. 4a. The inverse relationship between dust enrichment and pressure seen for chondrule enrichment in Section 2 is also seen here for CI dust enrichment, but only at relatively high pressure. The CI dust enrichment needed to retain 90% of the sodium at the highest temperature of olivine stability is seen to fall from $\sim 3 \times 10^4\times$ at $P^{tot} = 0.6$ bar to $\sim 300\times$ at 30 bars. For 50% sodium retention, the needed dust enrichment is only $\sim 1200\times$ at 0.6 bar and falls to $\sim 70\times$ at 30 bars. For both degrees of sodium retention, however, the curves turn upward, becoming vertical at P^{tot} of 0.5 and 4.7×10^{-2} bar for 90% and 50% sodium retention, respectively. At P^{tot} below these values, the respective degrees of sodium retention cannot be achieved at the maximum temperature of olivine stability regardless of the magnitude of dust enrichment. The dust enrichments corresponding to these limiting values of P^{tot} are $\sim 10^6\times$.

The reason why the behavior is so different from the chondrule enrichment case in Section 2 lies not in the dust composition but in the treatment of the pressure variable. At the maximum temperature of olivine stability, volatile S species, some of the sodium and, in the CI chondrite case, a large amount of water initially present in the dust are present in the ambient gas, which originally consisted only of the gas remaining after condensation of the dust from solar composition at some low temperature. In the chondrule enrichment case, the pressure variable is P^{tot}_H, which is held constant for each calculation of P^a_{Na} despite the addition of volatile species to the ambient gas mix. This causes P^{tot} to increase with increased sodium evaporation in Fig. 2. In the CI chondrite calculation, however, it is the total pressure, P^{tot}, that is assumed to be fixed for calculation of P^a_{Na}. Fig. 5 shows why this makes a difference. In it, the partial pressures of some important species in the ambient gas are plotted as a function of dust enrichment for the case of 50% sodium retention at the maximum temperature of olivine stability. At low dust enrichment, the high-temperature ambient gas speciation resembles that of the residual solar nebular gas. As the assumed value of P^{tot} is decreased, the dust enrichment needed for 50% sodium retention gradually increases, and matter devolatilized from this dust gradually becomes dominant in the ambient gas, causing, for example, the dramatic dilution of He. The relatively small decline in P^a_{Na} with increasing dust enrichment seen in Fig. 5 is due to a gradual fall in the incoming temperature of olivine which, in turn, causes a decline in P^v_{Na} which must be matched exactly by P^a_{Na} when 50% of the sodium is lost at this temperature. At a CI dust enrichment of $\sim 10^6\times$, a condition of infinite dust enrichment is reached, where the gas composition essentially becomes that of the devolatilized matter and thus remains fixed no matter how much additional dust is partially volatilized. At CI dust enrichments $\geqslant 10^6\times$, P^a_{Na} is simply the mole fraction of sodium in the devolatilized gas, multiplied by P^{tot}. Because this product is always less than the value of P^v_{Na} at the olivine incoming temperature for all $P^{tot} < 4.7\times 10^{-2}$ bar, the value corresponding to a CI dust enrichment of $10^6\times$, sodium cannot be retained after only 50% loss, and the curve on Fig. 4a turns sharply upward.

Alexander and Ebel (2012) employed yet a third technique for deriving the dust enrichment necessary for sodium retention. Because they calculated P^v_{Na} at fixed P_{H_2}, their technique is more closely related to that in Section 2 of the present work, and would have yielded similar results had the same f_{O_2} and dust composition been used, and if allowance had been made for the presence of abundant He in the ambient gas.

3.2.2. Oxygen fugacity of systems enriched in CI dust

Ebel and Grossman (2000) showed that the f_{O_2} of dust-enriched systems at a given temperature increases with increasing dust enrichment but is relatively insensitive to P^{tot}. Thus, in the calculations summarized in Fig. 4, the f_{O_2} is nearly constant at constant dust enrichment regardless of P^{tot}. In Fig. 6, $\log f_{O_2} - \log$ IW at the incoming temperature of olivine is plotted as a function of enrichment in CI and H′ dust for conditions along the 50% sodium retention curves of Fig. 4. As seen below, $\log f_{O_2} - \log$ IW varies by <0.2 between the maximum stability temperature of olivine and 1300 K for a given dust enrichment, so the variations seen in Fig. 6 are due almost entirely to the variation of P_{H_2O}/P_{H_2} with dust enrichment seen in Fig. 5, rather than temperature effects. Inspection of Fig. 6 reveals that droplets that form under conditions where 50% of the sodium is retained at the maximum temperature of olivine stability do so at progressively higher values of $\log f_{O_2} - \log$ IW with increasing dust enrichment, ranging, in the case of CI dust, from -2 to 0 as dust enrichment rises from 300 to $10^4\times$, and leveling off at $+0.5$ at infinite dust enrichment. Because the silicate fraction of the droplets is in equilibrium with coexisting metallic NiFe, this causes the mol% fayalite of the highest-temperature olivine that forms to increase with increasing dust enrichment, as indicated by the numbers along each of the curves in Fig. 4. In particular, for 50% sodium retention at the maximum temperature of olivine stability, the fayalite content of the first-formed olivine ranges from 0.6 mol% at a CI dust enrichment of $60\times$ to 8.2 mol% at $1 \times 10^4\times$, while the incoming temperature of olivine varies from 1950 to 1880 K. Fractional crystallization calculations like those in Fedkin et al. (2012) were used to calculate the mean fayalite content of olivine in droplets made from CI as well as from H′ dust. They show that the mean fayalite content

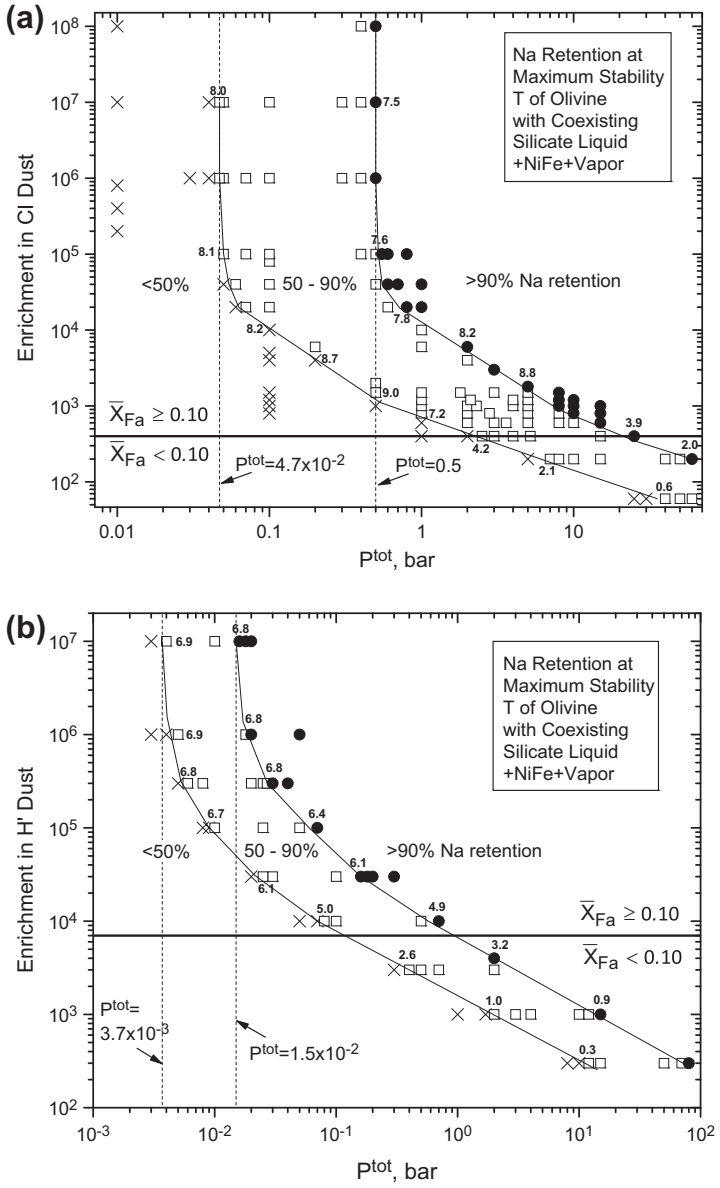

Fig. 4. Combinations of (a) CI and (b) H′ dust enrichment and P^{tot} at which the equilibrium condensation code was run. Circles, squares and crosses indicate conditions where >90%, 50–90% and <50%, respectively, of the sodium is condensed at the highest temperature of olivine stability. Interpolated curves are drawn to indicate conditions for 50% and 90% sodium retention. At $P^{tot} < 4.7 \times 10^{-2}$ bar, the gas can become saturated in sodium at the maximum temperature of olivine stability only when <50% of the sodium is retained, regardless of dust enrichment. Therefore, the 50% curve turns sharply upward at 4.7×10^{-2} bar. Horizontal lines separate fields where fractional crystallization leads to mean $X_{Fa} < 0.1$ and $\geqslant 0.1$. Numbers along curves are, in contrast, mol% fayalite of the initial, highest-temperature olivine. Silicate liquid, metallic nickel–iron and vapor are coexisting phases in all cases.

also increases with increasing dust enrichment. In Fig. 4a, a horizontal line is drawn at a CI dust enrichment of 400× to distinguish droplets whose olivine has a mean X_{Fa} characteristic of Type II chondrules, $\geqslant 0.10$, from those of Type I chondrules, <0.1.

3.2.3. Mineralogical and chemical evolution of a droplet that formed under conditions for 54% sodium retention

The high-temperature equilibrium phase assemblage is the same for all points on Fig. 4a. To illustrate the temperature variation of the equilibrium phase assemblage for a case of 54% sodium retention at the maximum stability temperature of olivine, the case of 800× CI dust enrichment at $P^{tot} = 1$ bar was selected for Fig. 7. It shows the distribution of iron between condensed phases and vapor over the temperature interval 2000–1200 K. At the maximum temperature of olivine stability, 1910 K, <1% of the iron is gaseous and the condensed iron is almost equally distributed between a ferromagnesian silicate liquid and a metallic NiFe alloy. As the temperature falls, olivine is the first phase to crystallize from the liquid; thus, the maximum temperature of olivine stability is the liquidus of the drop-

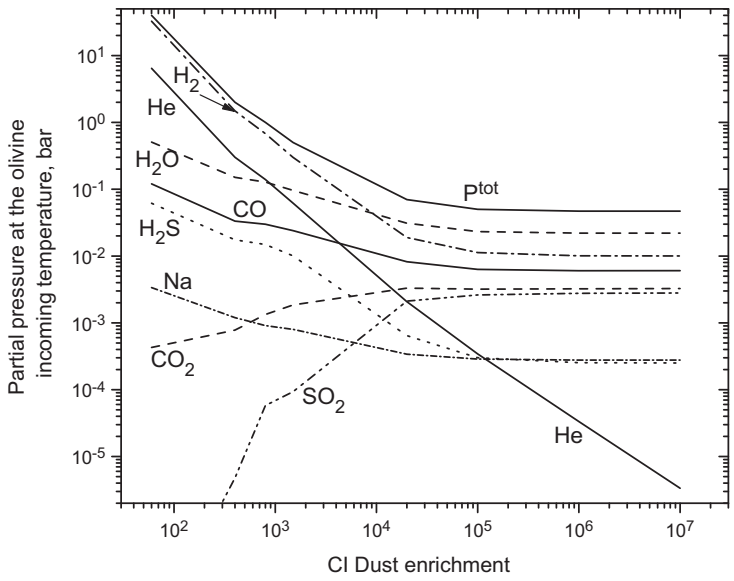

Fig. 5. Partial pressures of some important species in the ambient gas for the case of ~50% sodium retention at the maximum temperature of olivine stability. With increasing CI dust enrichment, volatiles degassed from CI dust gradually become dominant over the original, residual nebular gas. A condition of infinite dust enrichment is reached at $\sim 10^6\times$ where the gas composition becomes essentially invariant regardless of dust enrichment.

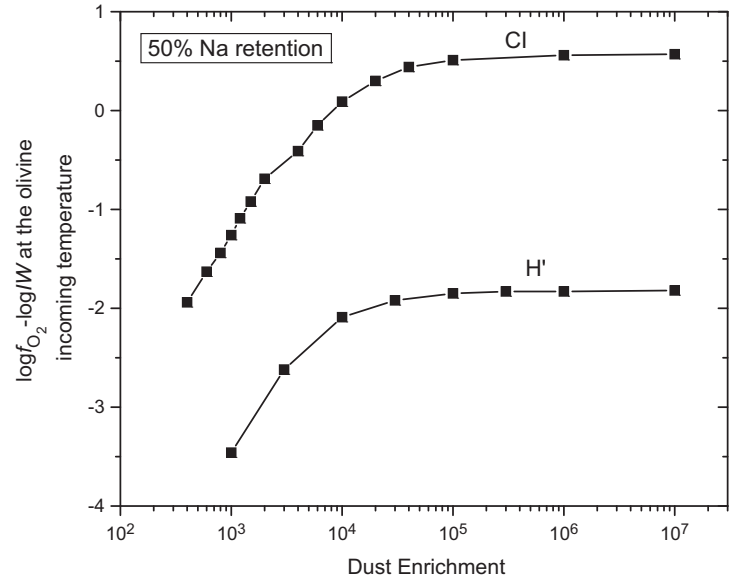

Fig. 6. Variation of log f_{O_2} − log IW with CI and H′ dust enrichment at the incoming temperature of olivine under conditions where ~50% of the sodium is retained at that temperature. Both curves level off at infinite dust enrichment. The difference between the curves is primarily due to the fact that much less water is devolatilized from H′ than from CI dust. The increase in f_{O_2} with increasing dust enrichment is the primary reason for the general increase in the initial fayalite content of olivine with increasing dust enrichment along each of the curves in Fig. 4a and b.

let. Olivine continues to crystallize with continued cooling, and is joined by a small amount of spinel at 1670 K. This spinel, with ~0.4–0.7 cations Mg, 0.2–0.6 cations Fe^{2+}, 1.3–1.6 cations Cr and 0.3–0.6 cations Al per 4 oxygen anions, is richer in Mg and Al and poorer in Fe than the chromite typical of Type II chondrules in Semarkona (Johnson and Prinz, 1991). This discrepancy may be due to the fact that coexisting olivine in the chondrules contains small amounts of Cr. The MELTS model does not allow for Cr substitution into olivine or pyroxene, causing the variation of the Cr content of the liquid to differ from that in natural chondrules.

The ratio of oxidized to reduced iron first decreases and then increases between the temperatures of appear-

ance of olivine and sulfide due to the temperature variation of the redox equilibrium between silicate liquid and metallic NiFe. Pyrrhotite is the sulfide predicted to form when metallic iron begins to react with gaseous sulfur at 1600 K. This is well above the minimum melting temperature in the Fe–Ni–S system, ~1262 K, so the calculated assemblage of pyrrhotite + metallic NiFe is metastable with respect to a metallic NiFe alloy and an Fe–S liquid. As in the work of Ebel and Grossman (2000), prediction of this metastable assemblage occurs because the computer code does not contain a thermodynamic model for Fe–Ni–S liquids. Because of this and the fact that, in many cases, VAPORS begins to display poor convergence at temperatures above that where sulfur is completely condensed, the Ni contents of metal grains that equilibrated with the silicate droplets at the temperature of complete condensation of sulfur had to be approximated. This was done by estimating the temperature of complete condensation of sulfur and determining the fraction of the iron that is oxidized at that temperature by extrapolating curves such as those in Fig. 7, and assuming that all S is FeS and all Ni is metallic.

Further insight into the evolution of this droplet is provided in Fig. 8, which shows the mineralogical and chemical changes in the silicate portion. When olivine begins to crystallize from the liquid, its composition is Fa_5, the log f_{O_2} is IW-1.57, 54% of the sodium is condensed and the liquid contains 0.5 wt.% Na_2O. By 1340 K, 76% of the liquid has crystallized as olivine whose equilibrium composition is Fa_{24}, the log f_{O_2} is IW-1.43, all the remaining sodium has condensed and the liquid contains 5.7 wt.% Na_2O. If most of the relatively large amounts of metallic NiFe ± iron sulfide with which the silicate portion equilibrated formed separate droplets, the object described here would closely resemble a Type II PO chondrule.

3.2.4. Bulk compositions of droplets that formed with ~50% sodium retention: Comparisons to Type II chondrules

The temperature variation of the bulk chemical composition of the silicate portions of droplets that form under conditions where ~50% of the sodium is condensed at the maximum temperature of olivine stability is shown in Fig. 9. Also plotted for comparison on this and many ensuing figures are the bulk compositions of individual Semarkona chondrules of the major types, and their glasses, from Jones and Scott (1989) and Jones (1990, 1994, 1996). Bulk and glass composition data obtained by Tachibana et al. (2003) and Kita et al. (2010) for Semarkona, Bishunpur and Krymka chondrules yield similar comparisons. On these figures, compositions of Types IB and IIB chondrules are included with those of Types IAB and IIAB, respectively, for simplicity. The model cases presented in Fig. 9 are for CI dust enrichments at 400×, 800×, and 1500× at P^{tot} of 2, 1 and 0.5 bar, where 46%, 54% and 51% of the Na is retained, respectively. The 800× case is the one shown also in Figs. 7 and 8. In Fig. 9, only the portions of the curves for temperature ranges below the incoming temperature of olivine are relevant because that is the peak temperature to which the porphyritic chondrule precursor was heated. Because Ca, Al, Mg and Si are nearly totally condensed below this temperature, the relative proportions of their oxides at each point along the calculated paths are nearly the same as in the starting material in column 1 of Table 2. Thus, the total variation in calculated bulk compositions in Fig. 9 is due only to FeO, whose concentration first decreases and then increases with falling temperature due to equilibration with coexisting metallic NiFe, and to alkalis, whose concentrations change due to their continued condensation. In the metal phase, X_{Ni} calculated at the incoming temperature of olivine and estimated at the

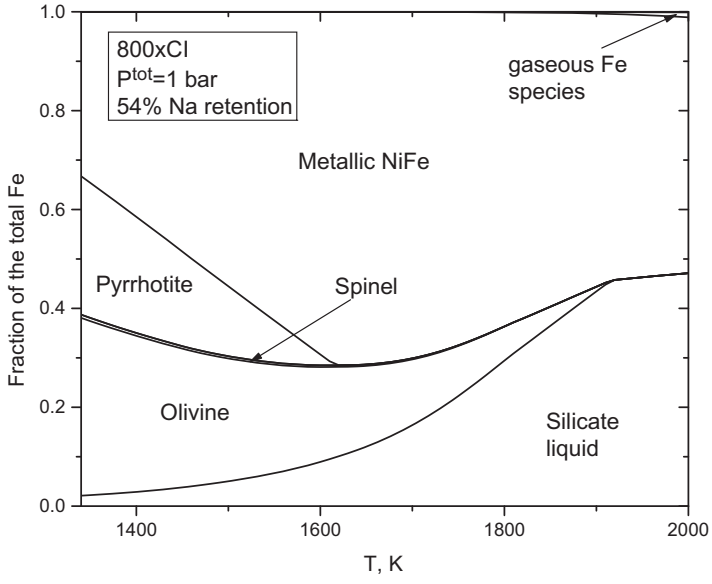

Fig. 7. Equilibrium distribution of iron calculated for a system enriched in CI dust by a factor of 800× relative to its complementary gas at $P^{tot} = 1$ bar. Olivine, the liquidus phase, begins to crystallize at 1910 K, where 54% of the sodium is condensed. At this temperature, iron is virtually totally condensed. The assemblage pyrrhotite ($Fe_{0.877}S$) + metallic NiFe calculated to exist between 1600 and 1200 K is metastable relative to metallic NiFe+ an Fe–S liquid at these conditions.

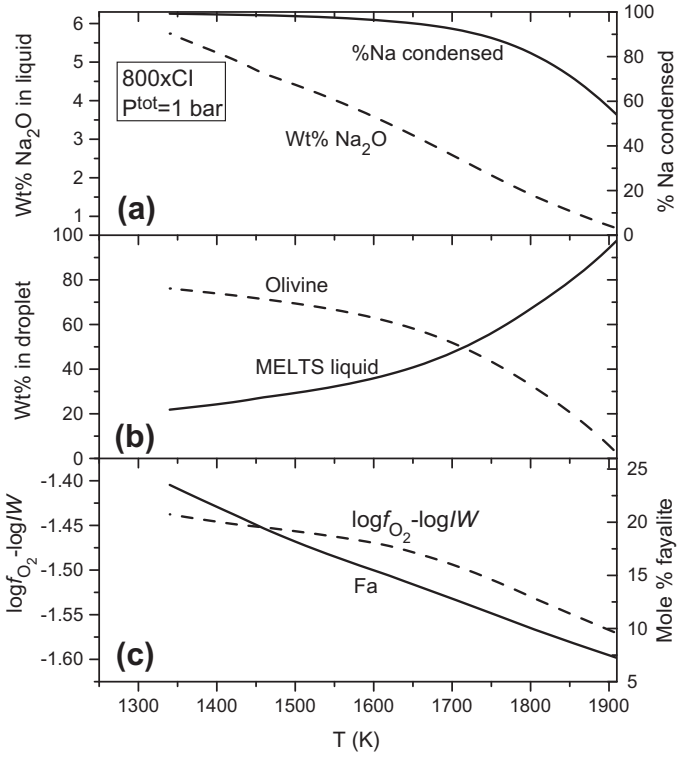

Fig. 8. Calculated mineralogical and chemical evolution of the silicate portion of a droplet that formed at a CI dust enrichment of 800× and $P^{tot} = 1$ bar, a case where 54% of the sodium is condensed at the maximum temperature of olivine stability. Crystallization of pyroxenes is suppressed. During cooling from 1910 to 1340 K, olivine reaches 76 wt.% of the silicate as its equilibrium fayalite content rises from 7 to 24 mol%, and the remainder of the sodium condenses, causing the wt.% Na_2O in the liquid to rise from 0.7 to 5.7 wt.%. The result closely resembles a Type II PO chondrule.

temperature of complete condensation of sulfur is 0.06 and 0.24, 0.09 and 0.65, and 0.17 and 0.73 at CI dust enrichments of 400×, 800× and 1500×, respectively. Increases in the initial and final FeO contents of the model droplets are seen with increasing dust enrichment. Droplets that form at CI dust enrichments between 400× and 800× at P^{tot} of 2 and 1 bar, respectively, have bulk compositions that come closest to those of Types IIAB and IIA chondrules. Those at the lower end of that range of dust enrichment lie closest to the lowest-FeO members of the Type IIAB group (Jones, 1996) and those at the upper end of the range of dust enrichment lie closest to the compositions of the Type IIAs (Jones, 1990). The path for 1500× is too FeO-rich to be a match for Type II chondrules.

The concentrations of Na_2O and FeO are plotted against one another in Fig. 10a, in which bulk compositions of model droplets are compared to those of natural chondrules. Once again, the paths for CI dust enrichment between 400× and 800× at P^{tot} of 2 and 1 bar, respectively, come closest to the range of FeO contents of Type II chondrules, with those at the lower end of the range of dust enrichment closest to the lowest-FeO members of the Type IIAB group and those toward the high end of the range of dust enrichment lying closest to the Type IIAs. The model curve for pure CI dust at 4.7×10^{-2} bar, the limiting P^{tot} for infinite dust enrichment, is seen to lie at an FeO content not far beyond that for 1.5×10^{3}×.

The paths for the 400–800× range of dust enrichment all end at Na_2O contents of 1.3–1.4 wt.%, at which point the Na_2O/SiO_2 ratio is solar, the only possible outcome when the precursor solid is assumed to have a solar ratio and the droplet acts as a closed system for these elements while molten. This assumption appears to be correct for the average Type IIAB chondrule composition, which lies on the 400× path, but cannot account for the factor of five range of Na_2O contents observed within the Type IIAB chondrule group or the fact that most Type IIA chondrules, hence their average composition, have Na_2O/SiO_2 ratios that are larger than the solar ratio. Additional model runs were conducted that were identical to those at 400× and 800× except that the Na and K abundances in the starting material were doubled and reduced to half of those of the CI composition in Table 2. At 400× dust enrichment and $P^{tot} = 2$ bars, where 54% of the sodium was lost from the original CI composition at the incoming temperature of olivine, the ambient gas reached sodium saturation after 65% and 49% sodium loss from the low- and high-sodium compositions, respectively. At 800× dust enrichment at $P^{tot} = 1$ bar, the low- and high-sodium composition lost 53% and 36% of their sodium, respectively, compared to 46% for the original CI starting material. As can be seen from Fig. 10a, Na_2O–FeO evolution curves for the model droplets produced from low- and high-Na_2O starting compositions span nearly identical ranges of FeO contents as the model droplets made from the original CI starting

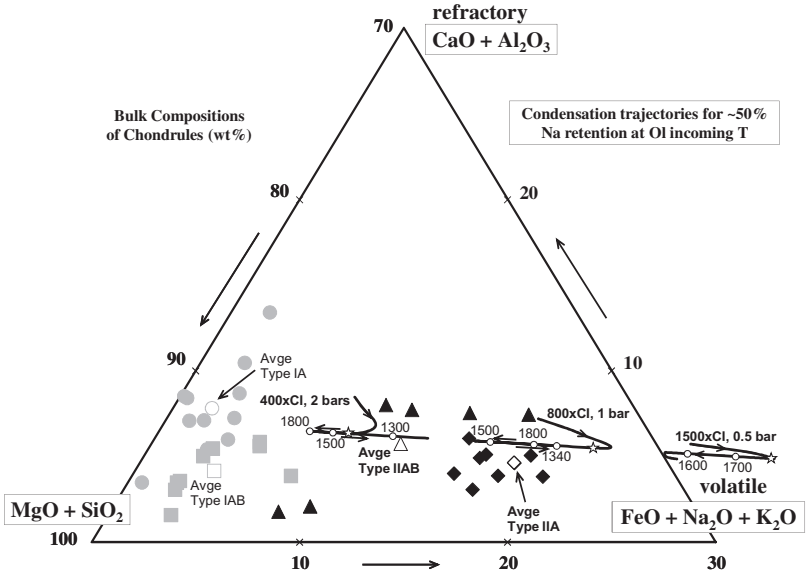

Fig. 9. Chondrule bulk compositions compared to paths of evolution of bulk chemical compositions of model droplets that formed under conditions of CI dust enrichment and P^{tot} where ~50% of the sodium was condensed at the maximum temperature of olivine stability. Numbers on curves are equilibration temperatures in K, and arrows show the direction of falling temperature. Only the part of each curve at temperatures below the olivine incoming temperature (open star) is relevant. Because Ca, Al, Mg and Si are fully condensed at this temperature, their inter-element ratios along the curves are fixed at values characteristic of the starting material (Table 2, column 1). Curves for dust enrichments between 400× (46% sodium retention) and 800× (54%) at $P^{tot} = 2$ and 1 bar, respectively, span the composition ranges of Types IIAB and IIA chondrules, whose symbols are black. Circles-Type IA; squares-Type IAB and IB; diamonds-Type IIA; and triangles-Type IIAB and IIB. Filled symbols – individual chondrule analyses; open symbols – group averages. See text for chondrule data sources.

material under the same conditions, but are displaced to lower and higher Na_2O contents, respectively. Thus, all Type II chondrule compositions, regardless of Na_2O content, could have formed at similar combinations of dust enrichment and P^{tot}, and with very similar degrees of sodium retention at the incoming temperature of olivine, provided they started with differing Na_2O contents inherited from a heterogeneous precursor.

Most Type I chondrules have Na_2O contents about a factor of two lower than the lowest Na_2O contents produced for Type II chondrules in the models considered in the above paragraph. If the Na_2O content of the CI parent material were slightly more heterogeneous than considered therein, it is conceivable that Type I chondrules could also be derived from such a parent. Inspection of Fig. 4a suggests that, starting with a CI parent, 50% sodium retention at the incoming temperature of olivine is possible under conditions where the highest-temperature olivine contains only 0.6 mol% fayalite. For this to occur, the CI material would have to be heated at dust enrichments of ~60× and P^{tot} ~40 bars, and the bulk FeO content of the droplet would be ~0.2 wt.%, similar to some Type I chondrules.

3.2.5. Evolution of liquid compositions in droplets that formed with ~50% sodium retention

Evolutionary paths of the chemical compositions of the silicate liquids are shown in Fig. 11a and b for model droplets that formed under conditions of CI dust enrichment and P^{tot} where ~50% of the sodium was condensed at the maximum temperature of olivine stability. The paths are compared with the glass compositions of the same chondrules whose bulk compositions were discussed in the previous section, and the data are from the same sources. As in the case of the bulk compositions of the model droplets, the liquids generally become more FeO-rich with increasing dust enrichment. The calculated paths in Fig. 11a are from runs in which pyroxenes were prevented from crystallizing, so the paths should be compared to compositions of glasses from Type IIA chondrules. The shapes of the paths are controlled in part by changes in bulk composition due to redox equilibration with metallic NiFe and recondensation of alkalis, but are mainly controlled by olivine subtraction, the net effect of which is progressive enrichment of the liquid in FeO and Na_2O at high temperature, and of CaO and Al_2O_3 at relatively low temperature. Calculated liquid compositions for a CI dust enrichment of 800× at $P^{tot} = 1$ bar pass directly through the cluster of Type IIA chondrule glasses, while the paths at 400× and 1500× are too low and too high, respectively, in FeO. Thus, the same set of conditions yield the best fits to both the liquid and the bulk compositions. Liquid compositions at specific temperatures along the 800× path are also listed in Table 3, where the similarity to the glass in Type IIA chondrule C71 of Jones (1990) can be seen.

Because pyroxenes were allowed to form in the runs whose liquid paths are plotted in Fig. 11b, these should be compared to glass compositions from Type IIAB chondrules. The high-temperature portions of these paths are identical to those in Fig. 11a but the low-temperature ends are affected by crystallization of pyroxenes, which causes the paths for all three dust enrichments to converge toward the cluster of glass compositions of Type IIAB chondrules. Orthopyroxene crystallizes at 1600 and

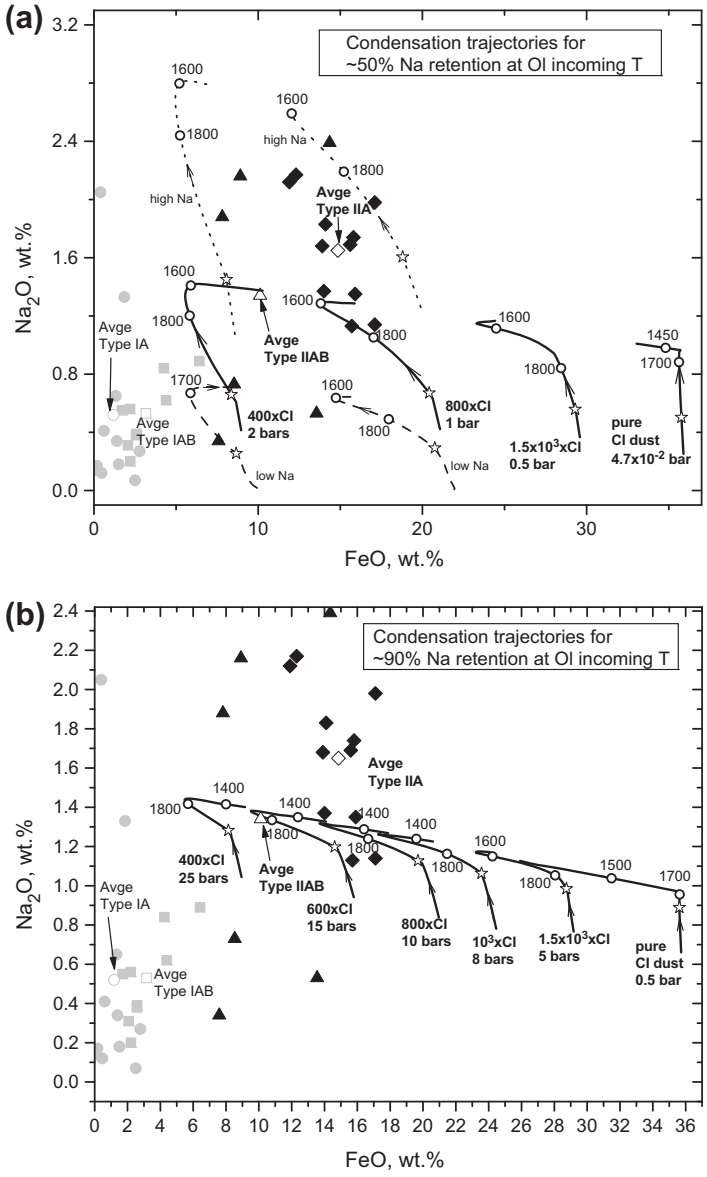

Fig. 10. Na_2O and FeO concentrations in chondrule bulk compositions compared to those along paths of evolution of bulk chemical compositions of model droplets that formed under conditions of CI dust enrichment and P^{tot} where (a) ~50% and (b) ~90% of the sodium was condensed at the maximum temperature of olivine stability. Only the part of each curve at temperatures below the olivine incoming temperature is relevant. Paths for pure CI dust at the limiting P^{tot} for infinite dust enrichment are also shown. Curves for dust enrichments between 400× and 800× at (a) $P^{tot} = 2$ and 1 bar, and (b) $P^{tot} = 25$ bars (90% sodium retention) and 10 bars (91%), respectively, lie closest to the compositions of Types IIAB and IIA chondrules, whose symbols are bold. At 400× and 800× in (a), dashed and dotted curves labeled low Na and high Na, respectively, are for model droplets made from starting compositions that have half of and double the Na_2O content of the CI starting composition in Table 2. Numbers on curves, symbols and data sources as in Fig. 9.

1450 K for the 400× and 800× cases, respectively, but not for the 1500× case. Clinopyroxene begins to crystallize at 1430, 1410 and 1380 K for the 400×, 800× and 1500× cases, respectively. The decrease in pyroxene incoming temperature with increasing dust enrichment is caused by an increase in the (Mg + Fe)/Si ratio of the silicate part of the system, which stabilizes olivine relative to pyroxene. Except for increasing FeO content with increasing dust enrichment, the clinopyroxene composition trends are similar for all three cases. For the 800× case, for example, the SiO_2, Al_2O_3, FeO, MgO and CaO contents in clinopyroxene vary from 53.8 to 52.2, 2.1 to 4.8, 6.7 to 4.6, 19.0 to 15.4, and 18.1 to 21.1 wt.%, respectively, as the temperature falls from 1410 to 1150 K. The high CaO and Al_2O_3 contents cause depletion of the liquid in $CaO + Al_2O_3$ during clinopyroxene crystallization. The similarity in composition between specific liquid compositions along the 800× path, especially that for 1450 K, and the glass in Type IIAB chondrule C190 of Jones (1996) can be seen in Table 3.

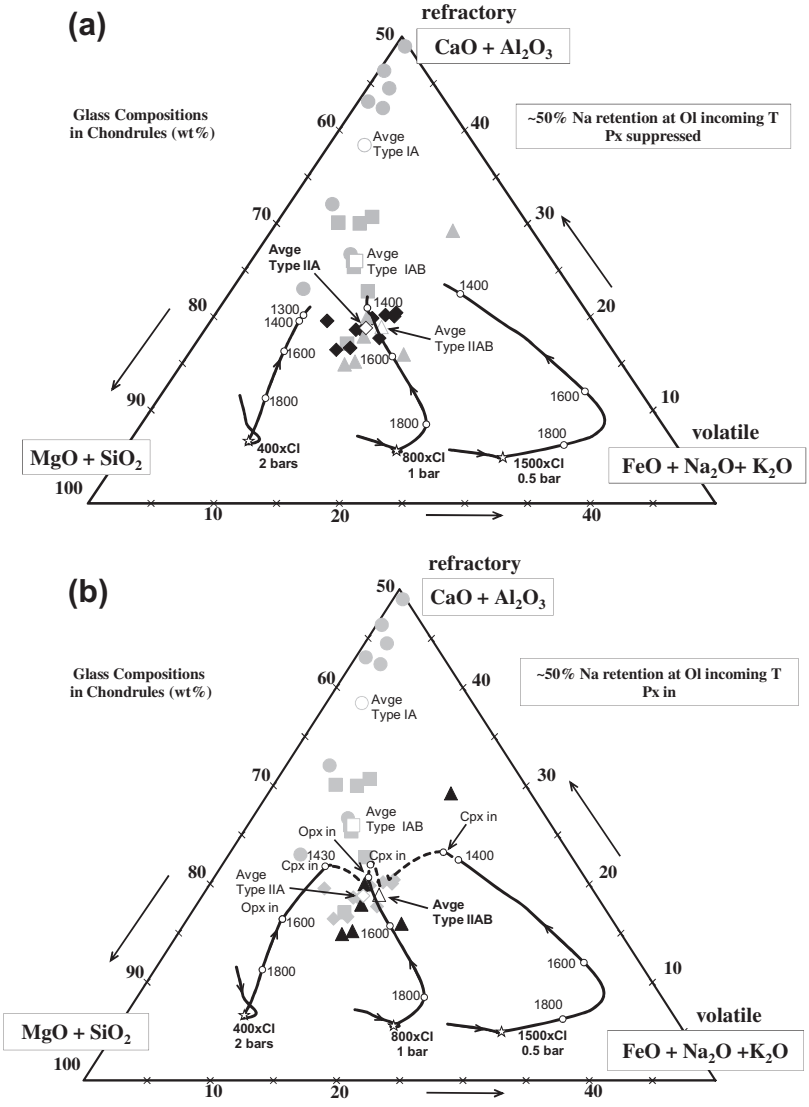

Fig. 11. Chondrule glass compositions compared to paths of evolution of chemical compositions of the silicate liquid portions of model droplets that formed under conditions of CI dust enrichment and P^{tot} where ~50% of the sodium was condensed at the maximum temperature of olivine stability. (a) Model curves from runs in which pyroxene formation was suppressed. Curves end where olivine crystallization ceases. The curve for CI dust enrichment of 800× at $P^{tot} = 1$ bar passes directly through the cluster of Type IIA glasses, whose symbols are bold. (b) Model curves from runs in which pyroxenes were allowed to crystallize. Dashed extensions were calculated using the MELTS model, and end where pyroxene crystallization ceases. The curves for all three dust enrichments converge on the cluster of Type IIAB glasses, whose symbols are bold. "Opx in" and "Cpx in" mark the incoming temperatures of orthopyroxene and clinopyroxene, respectively. Numbers on curves, data sources and other symbols as in Fig. 9.

3.2.6. Bulk compositions of droplets that formed with ~90% sodium retention

The bulk chemical compositions of Type II chondrules are equally well matched by droplets that formed under conditions of ~90% sodium retention at the maximum temperature of olivine stability, as seen in the Na_2O–FeO plot (Fig. 10b). Just as in the case of 50% sodium retention, the curves for CI dust enrichments of 400× and 800× bracket the range of FeO contents of Type II chondrules but the values of P^{tot} needed to achieve 90% and 91% sodium retention are 25 and 10 bars, respectively, ~10 times larger than the total pressures needed to achieve 50% retention. Ninety percent sodium retention can be achieved at lower values of P^{tot}, e.g., 0.5–8 bars, but the higher dust enrichments needed to reach this condition result in FeO contents $\geqslant$18 wt.%, higher than the bulk compositions of most Type II chondrules. The curve for infinite dust enrichment, at a P^{tot} of 0.5 bar, yields a final bulk FeO content for the droplet that is only slightly higher than that for $1.5 \times 10^3\times$.

3.3. Mixtures of residual nebular gas with heated H′ material

3.3.1. Conditions for sodium retention at the maximum temperature of olivine stability

Results for H′ dust are shown in Fig. 4b. As in the case of CI dust, for a given degree of sodium retention at the

Table 3
Model liquid compositions compared to glass compositions in selected chondrules (wt.%).

Model	800× CI; $P^{tot} = 1$ bar						
Conditions	Pyroxene suppressed			Pyroxene in			
T (K)	1910	1340		1450	1410	1140	
	Ol in	End		Opx in	Cpx in	End	
			IIA, C71[a]				*IIAB, C190*[b]
SiO_2	41.96	60.90	*61.60*	58.89	58.89	58.62	*61.10*
TiO_2	0.14	0.52	*0.44*	0.49	0.53	0.35	*0.44*
Al_2O_3	3.10	13.02	*11.20*	11.52	12.57	15.22	*11.40*
Cr_2O_3	0.66	0.05	*0.17*	0.10	0.07	0.01	*0.58*
Fe_2O_3	0.17	0.00	–	0.16	0.14	0.03	–
FeO	20.58	4.45	*7.85*	6.34	5.18	0.99	*8.30*
MnO	0.48	2.20	*0.22*	1.91	2.14	7.60	*0.67*
MgO	29.72	3.16	*3.42*	5.79	4.80	1.18	*4.10*
CaO	2.45	8.21	*8.62*	8.40	8.52	3.51	*7.80*
Na_2O	0.69	5.74	*5.18*	4.93	5.51	8.96	*3.00*
K_2O	0.04	0.57	*0.31*	0.48	0.54	1.65	*0.46*
P_2O_5	0.00	1.14	*1.54*	0.95	1.06	1.73	–
H_2O	0.01	0.03	–	0.03	0.04	0.13	–
Sum	100.0	100.0	*100.6*	100.0	100.0	100.0	*97.9*

Model	$4 \times 10^3 \times$ H′; $P^{tot} = 2$ bar							
Conditions	Pyroxene suppressed			Pyroxene in				
T (K)	1920	1390		1800	1410	1300	1150	
	Ol in	End		Opx in	Cpx in		End	
			IA, A81[c]					*IAB, C50*[d]
SiO_2	54.87	75.29	*65.50*	61.35	56.55	57.35	56.14	*59.70*
TiO_2	0.19	0.46	*0.51*	0.28	0.90	0.56	0.24	*0.54*
Al_2O_3	3.32	8.14	*14.50*	5.01	14.66	16.26	15.75	*17.20*
Cr_2O_3	0.24	0.23	*1.18*	0.56	0.11	0.05	0.03	*0.41*
Fe_2O_3	0.00	0.00	*0.00*	0.00	0.01	0.01	0.00	–
FeO	3.99	0.64	*0.35*	2.93	0.68	0.36	0.15	*3.50*
MnO	0.48	1.21	*0.14*	0.73	3.72	6.68	9.96	*0.53*
MgO	33.69	5.79	*4.56*	24.28	6.77	3.65	1.87	*3.70*
CaO	2.69	6.56	*8.08*	4.03	10.67	6.33	4.39	*7.80*
Na_2O	0.46	1.27	*4.47*	0.74	3.78	6.37	8.11	*3.80*
K_2O	0.05	0.13	*0.72*	0.07	0.39	0.70	1.04	*0.49*
P_2O_5	0.00	0.27	–	0.00	1.73	1.63	2.25	–
H_2O	0.02	0.02	–	0.02	0.03	0.05	0.08	–
Sum	100.0	100.0	*100.0*	100.0	100.0	100.0	100.0	*97.7*

[a] Data sources: Jones (1990).
[b] Data sources: Jones (1996).
[c] Data sources: Jones and Scott (1989).
[d] Data sources: Jones (1994).

maximum temperature of olivine stability, an inverse relationship exists between dust enrichment and P^{tot} at relatively high P^{tot}. For 90% sodium retention, the needed H′ dust enrichment is $\sim 5 \times 10^4\times$ at $P^{tot} = 10^{-1}$ bar and just $\sim$1200× at 10 bars. For 50% sodium retention, the required dust enrichments are ~8000× and ~300× at the same total pressures. Also as in the case of CI dust enrichment, a minimum value of P^{tot} exists below which a given degree of sodium retention cannot be achieved no matter how high the H′ dust enrichment. For 90% and 50% sodium retention, the minimum values of P^{tot} are 1.5×10^{-2} and 3.7×10^{-3} -bar, respectively, and the dust enrichment corresponding to these limiting values is $\sim 10^7\times$. The reason why the minimum values of P^{tot} are lower for H′ than for CI dust is that the concentrations of volatile water, sulfur and sodium are much smaller in H′ than in CI dust, requiring greater dust enrichments, and therefore lower P^{tot}, to dilute the original, residual nebular gas to a negligible fraction of the high-tem-

perature ambient gas. A manifestation of the lower water content of H′ dust is the fact that the f_{O_2} of the high-temperature ambient gas is ~2 log units lower for H′ dust than for the same enrichment in CI dust in Fig. 6. Because of this, the horizontal line separating the field where olivine has a mean X_{Fa} characteristic of Type II chondrules from that of Type I chondrules is at $7 \times 10^3\times$ H′ dust enrichment in Fig. 4b, much higher than for CI dust in Fig. 4a.

3.3.2. Mineralogical and chemical evolution of a droplet formed under conditions for 91% sodium retention

Details of the high-temperature silicate phase assemblage characteristic of the points in Fig. 4b are shown in Fig. 12 for an H′ dust enrichment of $10^3\times$ at $P^{tot} = 15$ bars, a case of 91% sodium retention at the maximum temperature of olivine stability. Olivine, $Fa_{0.9}$, begins to crystallize at 1930 K, where log f_{O_2} = IW-3.49, and there is 0.46 wt.% Na_2O in the liquid. By 1700 K, olivine whose equilibrium composition is $Fa_{1.5}$ makes up 45 wt.% of the droplet, the remainder of the sodium has condensed, and the liquid contains 0.92 wt.% Na_2O. At 1310 K, olivine, $Fa_{2.3}$, makes up 60% of the droplet, log f_{O_2} = IW-3.45 and the liquid is 1.25 wt.% Na_2O. If most of the relatively large amounts of metallic NiFe with which the silicate portion equilibrated formed separate droplets, the object described here would closely resemble a Type I PO chondrule. A small amount of spinel begins to crystallize from the liquid at 1570 K. Its composition, ~68 wt.% Cr_2O_3, 21% MgO, 9% Al_2O_3 and 2% FeO, is relatively invariant with temperature and is quite different from the nearly pure Mg-Al spinel in Murchison Type I chondrule 6–15 (Simon et al., 1994). Both the coexisting pyroxene (unpublished data from this laboratory) and olivine in this chondrule contain 0.1–0.2 wt.% Cr_2O_3, so the discrepancy between the spinel composition observed in this chondrule and that computed here may be due to the fact that MELTS does not allow for Cr substitution into either olivine or pyroxene.

3.3.3. Bulk compositions of droplets that formed with ~90% sodium retention: Comparisons to Type I chondrules

The temperature variations of the bulk chemical composition of the silicate portions of droplets that form under conditions where ~90% of the sodium is condensed at the maximum temperature of olivine stability are shown in Fig. 13. The three cases presented are for H′ dust enrichments of $10^3\times$, $4 \times 10^3\times$ and $10^4\times$ at P^{tot} of 15, 2 and 0.7 bar, where 91%, 91% and 92% of the sodium is retained, respectively. The $10^3\times$ case is the one shown also in Fig. 12. As in Fig. 9, only the portion of each curve at temperatures below the incoming temperature of olivine is relevant, and Ca, Al, Mg and Si are nearly totally condensed at these temperatures. Thus, at each point along the calculated paths, the relative proportions of these elements to one another are fixed at nearly the same values as those in column 2 of Table 2. Also as in Fig. 9, the total variation in calculated bulk compositions is in the $FeO + Na_2O + K_2O$ direction. In Fig. 13, these variations are very small because ~90% of the sodium is already condensed at the incoming temperature of olivine, and the total amount of FeO is quite small at the low oxygen fugacities of these runs (e.g., Fig. 12c). Because so little oxidation occurs and the Fe/S atomic ratios are so large in these systems, X_{Ni} in the coexisting metal phase is nearly invariant with temperature at 0.05–0.07 for all three dust enrichments. $CaO + Al_2O_3$ in the predicted bulk compositions is quite close to four out of nine of the Type IAB (Jones, 1994) and two out of eleven of the Type IA (Jones and Scott, 1989) chondrule compositions. Most of the remaining Type IAB and Type IA chondrules are substantially lower and substantially higher, respectively, in $CaO + Al_2O_3$ than predicted by the model. Given that these two oxides are totally condensed when sodium is 90%, or even 50%, condensed, the reported chondrule compositions can only be matched by the model if the starting material is heterogeneous in its $CaO + Al_2O_3$ values. Droplets that form at H′ dust enrichments between $10^3\times$ and $4 \times 10^3\times$ at P^{tot} of 15 and 2 bars, respectively, have bulk compositions that come closest to those of Types IA and IAB chondrules. The path for $10^4\times$ is too FeO-rich to be a match for most Type I chondrules.

Comparisons between the bulk compositions of model droplets and those of natural chondrules are best seen in Fig. 14a, where Na_2O and FeO are plotted against one another. As the temperature falls below the olivine incoming temperature, the FeO content is seen to increase monotonically at $10^3\times$, first decrease and then increase at $4 \times 10^3\times$ and decrease monotonically at the $10^4\times$ H′ dust enrichment. These relatively small variations are again due to the temperature variation of the redox equilibrium between the silicate and coexisting metallic NiFe. As also seen in Fig. 13, the FeO contents of most Type I chondrules are bracketed by the model curves at H′ dust enrichments of $10^3\times$ and $4 \times 10^3\times$, while the highest-FeO Type IAs might require an H′ dust enrichment as high as $10^4\times$.

The final Na_2O contents reached along these paths is 0.48 wt.%, consistent with complete condensation of all Na_2O in the H′ starting material. Additional model runs were conducted that were identical to those at $10^3\times$ and $4 \times 10^3\times$ except that the Na and K abundances in the starting material were doubled and reduced to half of those of the H′ composition in Table 2. At both dust enrichments, the ambient gas reached sodium saturation after 12% sodium loss from the low-sodium composition and after 7% loss from the high-sodium composition, compared to 9% loss from the original H′ composition, all at the incoming temperature of olivine. The Na_2O–FeO evolution curves for the model droplets produced from low- and high-Na_2O starting compositions are plotted in Fig. 14a, where they are seen to span nearly identical ranges of FeO contents as the model droplets made from the original H′ starting material under the same conditions, but are displaced to lower and higher Na_2O contents, respectively. Thus, despite the very large, factor of 29, variation in bulk Na_2O content seen in Type I, particularly Type IAB, chondrules, all of them could have formed at similar combinations of dust enrichment and P^{tot}, and with very similar degrees of sodium retention at the incoming temperature of olivine, provided they started with different Na_2O contents inherited from a heterogeneous precursor.

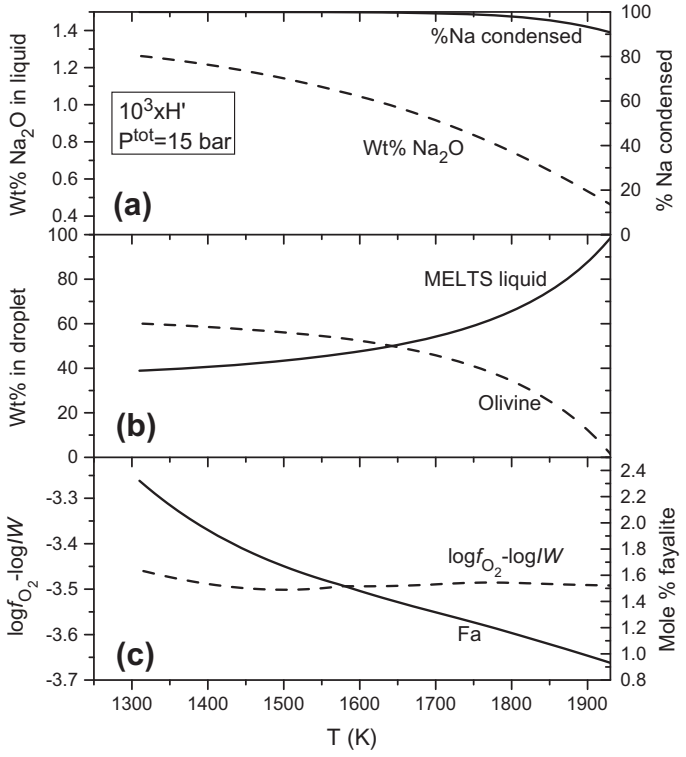

Fig. 12. Calculated mineralogical and chemical evolution of the silicate portion of a droplet that formed at an H′ dust enrichment of $10^3\times$ and $P^{tot} = 15$ bars, a case where 91% of the sodium is condensed at the maximum temperature of olivine stability. Crystallization of pyroxenes is suppressed. During cooling from 1930 to 1310 K, olivine reaches 60 wt.% of the silicate as its equilibrium fayalite content rises from 0.9 to 2.3 mol%. The remainder of the sodium condenses, causing the wt.% Na_2O in the liquid to rise from 0.45 to 1.25 wt.%. The result closely resembles a Type I PO chondrule.

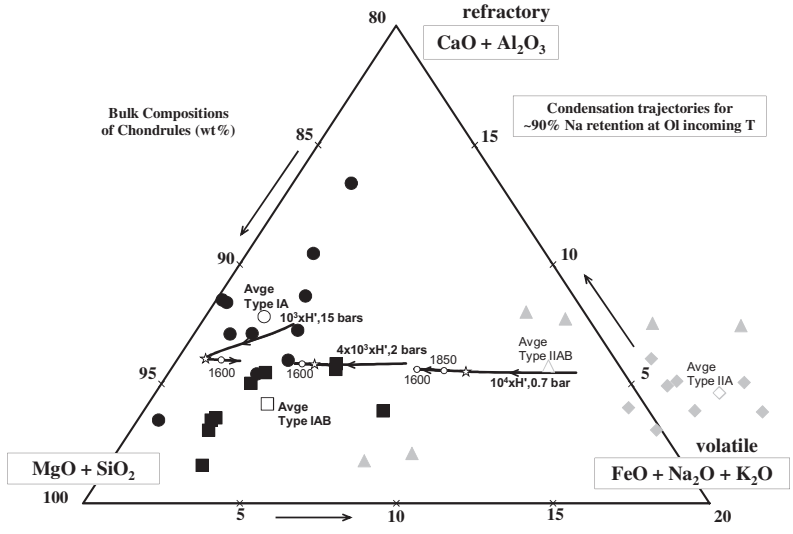

Fig. 13. Chondrule bulk compositions compared to paths of evolution of bulk chemical compositions of model droplets that formed under conditions of H′ dust enrichment and P^{tot} where ~90% of the sodium was condensed at the maximum temperature of olivine stability. Because all Ca, Al, Mg and Si are condensed at this temperature and below, their inter-element ratios along the curves are fixed at values characteristic of the starting material (Table 2, column 2). Curves for dust enrichments between $10^3\times$ and $4\times10^3\times$ at $P^{tot} = 15$ and 2 bars, respectively, for both of which 91% of the sodium is retained, come closest to the composition ranges of Types IA and IAB chondrules, whose symbols are bold. Numbers on curves, data sources and other symbols as in Fig. 9.

In Fig. 14a, it is noteworthy that the curve for infinite H′ dust enrichment, at $P^{tot} = 1.5 \times 10^{-2}$ bar, lies at an FeO content of ~15 wt.%. If some of the H′ starting material were as high in Na_2O as 2 wt.%, the compositions of many of the relatively low-FeO (7–15 wt.%) Type II chondrules in Fig. 14a could be accounted for by heating it at relatively low P^{tot} in the presence of relatively small amounts of residual nebular gas, e.g., dust enrichments from $10^4\times$ at $P^{tot} = 0.7$ bar to $10^7\times$ at $P^{tot} = 1.5 \times 10^{-2}$ bar.

3.3.4. Evolution of liquid compositions in droplets that formed with ~90% sodium retention

The evolution of the chemical composition of the silicate liquids is shown in Fig. 15a and b for model droplets that formed at H′ dust enrichments of 10^3, 4×10^3 and $10^4\times$ and P^{tot} of 15, 2 and 0.7 bar, respectively, conditions where ~90% of the sodium is condensed at the maximum temperature of olivine stability. The paths begin near the $MgO + SiO_2$ apex with ~3.0 wt.% Al_2O_3 and

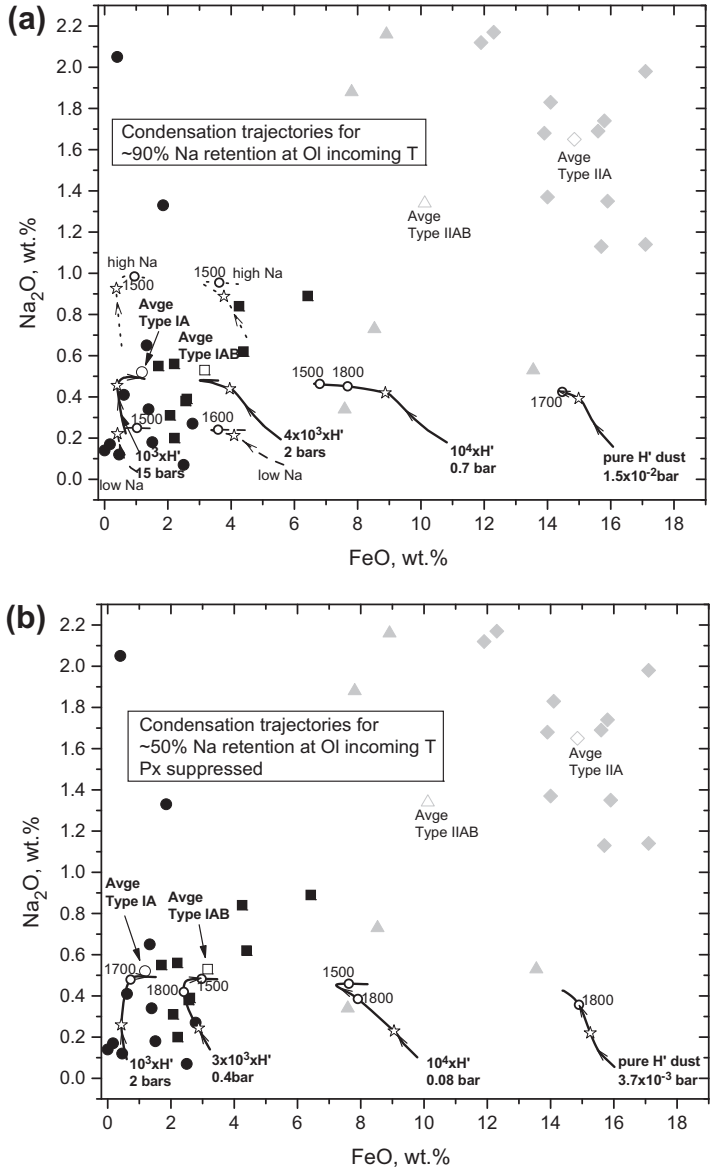

Fig. 14. Na_2O and FeO concentrations in chondrule bulk compositions compared to those along paths of evolution of bulk chemical compositions of model droplets that formed under conditions of H′ dust enrichment and P^{tot} where (a) ~90% and (b) ~50% of the sodium was condensed at the maximum temperature of olivine stability. Paths for pure H′ dust at the limiting P^{tot} for infinite dust enrichment are also shown. Curves for dust enrichments between (a) $10^3\times$ and $4 \times 10^3\times$ at $P^{tot} = 15$ and 2 bars, respectively, and (b) $10^3\times$ (51% sodium retention) and $3 \times 10^3\times$ (50%) at $P^{tot} = 2$ and 0.4 bar, respectively, span the range of FeO contents of most Types IA and IAB chondrules. At $10^3\times$ and $4 \times 10^3\times$ in (a), dashed and dotted curves labeled low Na and high Na, respectively, are for model droplets from starting compositions that have half of and double the Na_2O content of the H′ starting composition in Table 2. Numbers on curves, symbols and data sources as in Fig. 9.

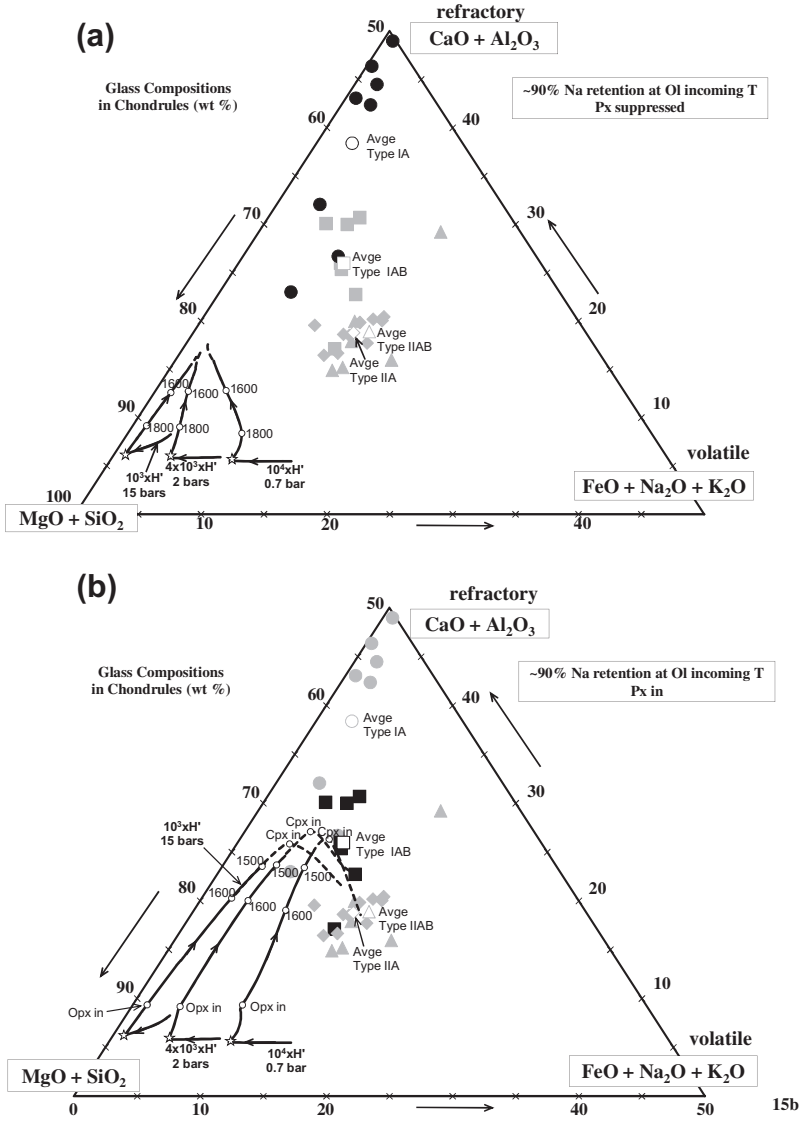

Fig. 15. Chondrule glass compositions compared to paths of evolution of chemical compositions of the silicate liquid portions of model droplets that formed under conditions of H′ dust enrichment and P^{tot} where ~90% of the sodium was condensed at the maximum temperature of olivine stability. (a) Model curves from runs in which pyroxene formation was suppressed. Dashed extensions were calculated using the MELTS model, and end where olivine crystallization ceases. Calculated liquid compositions do not show the extreme enrichment in $CaO + Al_2O_3$ exhibited by the Type IA glasses (black symbols), primarily because their parent chondrules contain considerably more of these oxides than is possible for model chondrules made from the solar composition starting material used here. (b) Model curves from runs in which pyroxenes were allowed to crystallize. Dashed extensions were calculated using the MELTS model, and end where pyroxene crystallization ceases. The curves for all three dust enrichments come closest to the Type IAB chondrules (black symbols) with the lowest $CaO + Al_2O_3$. Numbers on curves, data sources and other symbols as in Figs. 9 and 11.

~2.5 wt.% CaO, and FeO content increasing from 1 to 10 wt.% with increasing dust enrichment. Olivine begins crystallizing at 1930, 1920 and 1910 K at H′ dust enrichments of 10^3, 4×10^3 and $10^4\times$, respectively. When pyroxene crystallization is suppressed (Fig. 15a), progressive olivine subtraction and FeO reduction cause the paths to converge at low FeO and alkali contents, while the liquids become enriched in CaO and Al_2O_3. After ~60% olivine crystallization, the liquids reach ~15 wt.% $CaO + Al_2O_3$, which falls far short of the values reported for Type IA glass compositions by Jones and Scott (1989) in Fig. 15a. This discrepancy is also seen in Table 3, where the lowest-temperature liquid composition for the $4 \times 10^3\times$ model run can be compared to the glass with the lowest $CaO + Al_2O_3$ of all the Type IA chondrules of Jones and Scott (1989). Five of the eight glasses contain 40–50 wt.% $CaO + Al_2O_3$ and the other three contain 23–31% (Fig. 15a). In all cases but one, the discrepancy between model and observed glass compositions is due to much higher $CaO + Al_2O_3$ in the reported bulk chondrule compositions (from 6.8 to 12.5 wt.%) than what is possible for model droplets made from the solar

composition starting material in Table 2. In one chondrule, however, C61, $CaO + Al_2O_3$ is only 3.2 wt.% in the bulk composition and 48.1 wt.% in the glass (Jones and Scott, 1989). This implies that the broad-beam EPMA used for the bulk composition determination sampled more than 93 wt.% olivine, which is more than 10 wt.% higher than can crystallize from the measured bulk composition according to MELTS. Perhaps olivine is over-represented in the analyzed section of C61, and its bulk composition is actually higher in $CaO + Al_2O_3$ than the reported value.

When pyroxene is allowed to crystallize (Fig. 15b), the model liquid trends become much more enriched in $CaO + Al_2O_3$ than in the analogous cases where pyroxene is suppressed. Highlighted for comparison in Fig. 15b are the compositions of Type IAB glasses from Jones (1994). Two pyroxenes crystallize below the olivine incoming temperature: orthopyroxene at 1810, 1800 and 1770 K at H′ dust enrichments of 10^3, 4×10^3 and $10^4\times$, respectively; and clinopyroxene at 1410 K in all three cases. At its incoming temperature, clinopyroxene that forms at an H′ dust enrichment of $10^3\times$ and P^{tot} of 15 bars contains 54.6 wt.% SiO_2, 2.4% Al_2O_3, 0.7% FeO, 20.4% MgO and 21.6% CaO. Except for slightly increasing FeO content with increasing dust enrichment, the clinopyroxene composition varies little with dust enrichment or temperature. The relatively high CaO and Al_2O_3 contents of this phase cause $CaO + Al_2O_3$ along all three liquid trends in Fig. 15b to begin to decline after reaching values of 25–27 wt.%, where clinopyroxene crystallization begins. Thus, the calculated liquid trends fail to reach $CaO + Al_2O_3$ values of 29–30 wt.%, the highest values found in three of the glasses, but they pass very close to the compositions of three of the other four glasses with lower values. Details of the composition of one of the latter glasses, that from chondrule C50 of Jones (1994), are shown on Table 3, where it is seen to be in fairly good agreement with the liquid composition calculated at 1300 K for the $4 \times 10^3\times$ model run, except for the very high MnO in the latter. That discrepancy is due to the fact that VAPORS does not allow MnO substitution into olivine or pyroxene, thus allowing its concentration to build up in residual liquids.

3.3.5. Bulk compositions of droplets that formed with ~50% sodium retention

The bulk chemical compositions of Type I chondrules are equally well matched by droplets that formed under conditions of 50% sodium retention at the maximum temperature of olivine stability, as seen in the Na_2O–FeO plot (Fig. 14b). Just as in the case of 90% sodium retention, the curves for H′ dust enrichments of $10^3\times$ and $10^4\times$ bracket the range of FeO contents of Type I chondrules but the values of P^{tot} needed to achieve 51% and 50% sodium retention are 2 and 8×10^{-2} bar, respectively, ~10 times smaller than the total pressures needed to achieve 90% retention. Fifty percent sodium retention can also be achieved at higher values of P^{tot}, e.g., 3–10 bars, and the lower dust enrichments needed to reach this condition result in bulk FeO contents of ~1 wt.% in the droplet.

4. CHONDRULE FORMATION IN IMPACT-GENERATED PLUMES

4.1. When the target composition is CI chondrite

Hewins et al. (2012) found that ~50% of the sodium was retained by Type II chondrules at their peak temperatures, while Alexander et al. (2008) suggested that ~90% was retained by both Type I and Type II chondrules. Regardless of whether 10 or even 50% of the sodium was lost, it was shown in Section 3 that cessation of sodium evaporation by saturation of the ambient gas requires either very high P^{tot} or very high dust enrichments, or both. If an impact on a body of CI composition caused instantaneous heating, melting and devolatilization of the target material and ejection of a plume of gaseous, liquid and solid matter that mixed with residual nebular gas at conditions where 50% or 90% of the sodium was retained by the resulting droplets at their liquidus temperature, their mineralogical and chemical properties would strongly resemble those of Type II chondrules. If the droplets cooled and equilibrated with the mixture of residual nebular gas and their devolatilized water, sulfur and alkalis, the fayalite content of the olivine and the chemical compositions of the bulk droplets (Figs. 9 and 10) and their glasses (Fig. 11) would most closely resemble those of Types IIA and IIAB chondrules at CI dust enrichments between 400× and 800×. For 50% sodium retention, the corresponding values of P^{tot} are 2 bars (for 400×) and 1 bar (for 800×). For 90% retention, they are 25 and 10 bars, respectively (Fig. 10b).

The sodium retention condition can be met at lower values of P^{tot} than these (Fig. 4a) but the correspondingly higher dust enrichments would lead to bulk droplet FeO contents that are higher than those of the suites of chondrules plotted in Figs. 9 and 10. In particular, at the lower limit values of P^{tot} of 4.7×10^{-2} and 0.5 bar, corresponding to infinite dust/gas ratios for 50% and 90% sodium retention, respectively, the bulk FeO contents would be ~24 wt.%, quite a bit higher than the chondrules with the highest FeO contents plotted in Fig. 10. This would suggest that at least some small amount of residual nebular gas, corresponding to 400–800× CI dust enrichment, is required to mix with hot CI chondrite ejecta in order for the resulting mixture to be sufficiently reducing to yield the bulk FeO contents characteristic of Type II chondrules.

The sodium retention condition can also be met at higher values of P^{tot} than 1–2 bars (for 50%) and 10–25 bars (for 90%) but the correspondingly low CI dust enrichments, <400×, would lead to bulk FeO contents more typical of Type I chondrules. Because all of the model runs represented on Fig. 4a have solar atomic Na/Si ratios, however, they cannot reproduce the mean Type IA or IAB chondrule Na_2O content, which is more than a factor of three smaller than the mean Type II chondrule value. Nevertheless, there are two Type I chondrules with unusually high Na_2O contents plotted on Fig. 10a. One of these, with 1.3 wt.% Na_2O and 2 wt.% FeO, could probably be made from CI chondrite ejecta at a dust enrichment of ~300× and the P^{tot} corresponding to this dust enrichment for the appropriate degree of sodium retention.

4.2. When the target composition is ordinary chondrite-like

When an impact occurs on a body with an anhydrous, ordinary chondrite-like composition, such as H′, the ejected droplets are bathed in a gas mix consisting mostly of devolatilized sulfur and alkalis with residual nebular gas. The much lower water content than in the case of an impact on a CI-composition body results in a much more reducing plume. If the P^{tot} and dust enrichment conditions of the plume were such that 50% or 90% of the sodium were retained by the resulting droplets at their liquidus temperature, the mean fayalite content of the olivine and the chemical compositions of the bulk droplets (Figs. 13 and 14) and their glasses (Fig. 15) would most closely resemble those of Types IA and IAB chondrules at H′ dust enrichments between $10^3\times$ and $4\times10^3\times$. For 90% sodium retention, the corresponding values of P^{tot} are 15 bars (for $10^3\times$) and 2 bars (for $4\times10^3\times$). For 50% retention, they are 2 and 8×10^{-2} bars, respectively (Fig. 14b).

The sodium retention condition can be met at lower values of P^{tot} than these (Fig. 4b) and the correspondingly higher dust enrichments would lead to bulk FeO contents that are higher than those of the Type I chondrules in Fig. 14. In particular, at the lower limit values of P^{tot} of 3.7×10^{-3} and 1.5×10^{-2} bar, corresponding to infinite dust/gas ratios for 50% and 90% sodium retention, respectively, the bulk FeO contents would be ~15 wt.%, quite a bit higher than the Type I chondrules with the highest FeO contents but within the range of many relatively low-FeO Type II chondrules plotted in Fig. 14. Thus, in the case of impacts on a body of ordinary chondrite composition, the ejecta must mix with at least some residual nebular gas in order for the resulting droplets to have the FeO contents of Type I chondrules. If no mixing with residual nebular gas occurs, however, droplets having FeO contents like those of some Type II chondrules could result. While the Na_2O contents of most of the latter are higher than can be achieved by impacts on a body of H′ composition, there are three Type IIAB chondrules in Fig. 14 whose contents of both FeO and Na_2O are low enough that they could have formed in this way.

4.3. Variations on plume composition

In this work, the impact plume is assumed to be composed largely of ejecta from an ordinary chondrite-like object, H′, that often results in relatively reduced products, or from a CI chondrite, that often results in more oxidized material. When contemplating what sorts of products would result from impacts on bodies of other compositions, it is useful to think of the examples explored in this work as end-member cases. For example, if the plume were composed largely of ejecta from a CM chondrite, having a water content between that of an ordinary chondrite and a CI, the products would be intermediate in composition between those from a CI and an H′ plume at the same conditions. Similarly, if the plume were made largely of ejecta from an anhydrous object like a CV chondrite, the products would be closer to those in the H′ case.

The bulk composition of the plume has been considered to be that of the target throughout this work. This is equivalent to assuming that the impactor contributes an insignificant fraction of the plume matter or that the impactor has the same composition as the target. Alternatively, one could imagine circumstances under which a plume consists of subequal amounts of target and impactor materials of different compositions from one another. An impact between an H′ and a CI body, for example, would be expected to generate molten droplets having mineralogical and chemical properties intermediate to those of the end-member cases discussed herein.

4.4. Heterogeneity of target and plume

Rather large variations were noted above in the $CaO + Al_2O_3$ content of individual Type I chondrules. Because an element as volatile as sodium was largely retained, it is inconceivable that variations in abundances of refractory elements like Ca and Al were produced during chondrule formation. Therefore, the parent material of Type I chondrules was heterogeneous in its abundances of Ca and Al. The fact that these chondrule-to-chondrule variations in bulk chemical composition were inherited from their parent materials raises the question of the spatial scale of chemical heterogeneity on the impacted bodies. If mm-scale mineralogical heterogeneity existed on impacted bodies, and if each liquid droplet produced in an impact was generated from a restricted region whose dimensions were comparable to those of a chondrule, it is easy to see how the observed chondrule-to-chondrule variations in $CaO + Al_2O_3$ were produced. If, on the other hand, chondrules represent droplets fragmented from larger melt volumes that were instantaneously homogenized upon impact, chondrule chemical variations would have to reflect either mineralogical variations that existed on a correspondingly larger spatial scale on the impacted body or impacts on a wide range of bodies of different composition.

The Type I and Type II chondrules considered herein vary in their Na_2O content by factors of ~29 and ~7, respectively. It is difficult to see how such large, droplet-to-droplet variations in Na_2O content could have been inherited from heterogeneous parent materials and preserved. Unlike CaO and Al_2O_3, the Na_2O content of each chondrule fell by 10–50% during olivine crystallization, and then came into equilibrium with the ambient gas. It was shown in Section 3 that droplets starting with identical composition except for their Na_2O contents, and bathed in gases of the same P^{tot} and dust enrichment, would retain slightly different fractions of their sodium at peak temperature and, upon cooling, would re-inherit their different Na_2O contents but would otherwise be very similar in mineralogical and chemical composition. If, however, an array of such droplets produced by a single impact on a heterogeneous parent were placed in a common plume and equilibrated with a common gas composition under similar physico-chemical conditions, they would all end up with nearly uniform Na_2O contents, largely erasing their initial differences in the content of this oxide. In a mixture of initially low- and high-Na_2O droplets, the uniform Na_2O con-

tent reached at equilibrium would be closer to the initial Na_2O content of the low-Na_2O droplets when they dominate the mixture and closer to that of the high-Na_2O droplets when the latter dominate. If this happened, some chondrules would have undergone a net gain of Na_2O during melting; yet, mineral-chemical evidence for such objects has not yet been presented in the literature. Given the fact that each chondrule equilibrated its Na_2O content with its ambient gas, it is difficult to reconcile chondrule-to-chondrule variations in Na_2O content of factors of 7–29 with formation in a common plume. One way for an array of droplets produced in a single event to end up with the observed range of Na_2O contents is if the mean initial Na_2O content of the droplets and, consequently, P^a_{Na} varied from place to place within the plume. Such spatial heterogeneity could have arisen from spatial heterogeneity of the target or may reflect internal variations in the relative proportions of target and impactor materials. Given the rapid evolution of impact plumes, and processes within them that are capable of separating dust from gas, perhaps the spatial scale of such heterogeneities was as small as meters, rather than kilometers. The alternative to such a model for producing the large observed variations in Na_2O content from chondrule to chondrule within a single chondrite is multiple impacts on targets of different compositions.

4.5. Chondrites

Chondrules ultimately accreted together with many other components to form chondrites. In Allende, for example, chondrules are mixed together with coarse-grained CAIs, fine-grained inclusions, amoeboid olivine aggregates, large single olivine crystals and a matrix of fine-grained, very FeO-rich olivine. Some of these components are solar nebular in origin, with no history of residence in a pre-existing parent body; others are of unknown origin. While it is relatively straightforward to show that the chondrule population in a given chondrite class has a bulk composition different from that of the fine-grained matrix in the same class (e.g., Hezel and Palme, 2010), it is much more difficult to demonstrate complementarity, i.e., that the bulk composition of every carbonaceous chondrite class, representing the mean composition of all components, including chondrules and matrix, is quantitatively identical (Huss et al., 2005). Complementarity would imply that each carbonaceous chondrite class formed by representative sampling of multiple components from systems of uniform composition.

In the present work, chondrules are made in impact-generated plumes whose non-volatile element abundances are those of either a CI or an H chondrite. Because neither Mg nor Si evaporate in this model, the resulting chondrules are constrained to have the Mg/Si weight ratios of the compositions in Table 2, i.e., 0.929 and 0.820 for the CI and H′ plume, respectively. In Section 3, bulk compositions of model chondrules are compared to those of chondrules from Semarkona, an LL chondrite. This is justified by the fact that the mean Mg/Si weight ratio of all 124 chondrules from LL chondrites measured by Jones and Scott (1989), Jones (1990, 1994, 1996), Tachibana et al. (2003) and Kita et al. (2010) is 0.929, identical to the CI ratio and only 13% larger than the H chondrite ratio. The mean Mg/Si weight ratio of LL chondrite falls is 0.801 (Jarosewich, 1990), so the Mg/Si weight ratio in LL chondrules is 16% larger than that of bulk LL chondrites. From this, it is evident that the matrix of LL chondrites has a significantly lower Mg/Si ratio than LL chondrules. If the chondrules in LL chondrites formed by an impact on a body of CI composition, the fine-grained dust with which they mixed when accreting into the LL chondrite parent body cannot simply be the pulverized, less strongly heated dust from the same impact, as it has a different composition from the chondrules.

4.6. Constraints on physico-chemical conditions within the plume

If impacts were the heat source for the generation of molten chondrules, they must be able to satisfy the experimentally derived constraints on chondrule thermal history. Most chondrules were heated to near-liquidus temperatures and then cooled at ~10–100 K/h. The work presented here provides additional constraints on the P^{tot} and the proportion of dust relative to gas in the plume. What relative sizes and velocities of impactor and target bodies were necessary, what their porosities had to be and what angles of incidence were necessary to satisfy these constraints, and whether the appropriate impact conditions could have been met by an early population of carbonaceous and ordinary chondrite composition planetesimals embedded in residual nebular gas are questions that await detailed modeling.

In order to satisfy the sodium saturation and oxidation state constraints, it was shown above that values of P^{tot} ranging from 10^{-3} bar all the way up to 25 bars were necessary when PO chondrules were at their liquidus temperature. Recall that $P^a_{Na} = P^v_{Na}$ at that point, and that $P^a_{Na} \propto P^{tot}$. While there is little doubt that impact-generated gases can reach high P^{tot}, and therefore high P^a_{Na} under these circumstances, there remains the question of the length of time such pressures would be maintained. In Fig. 8, for example, equilibrium recondensation of sodium into a Type II chondrule occurred while the droplet cooled through ~500 K. If the droplet cooled at 10 K/h, for example, conditions for sodium recondensation had to persist in the impact plume for ~50 h. During this time, the P^{tot} and P^a_{Na} generated by the impact would have surely declined from their high initial values as the plume expanded and cooled. Had P^a_{Na} fallen below P^v_{Na}, the sodium saturation condition would have broken down, causing more sodium to evaporate. During cooling, however, P^v_{Na} over a typical chondrule composition also declines, by a factor of ~10 every 200 K. Thus, sodium evaporation would not have occurred upon cooling if P^{tot} fell by no more than a factor of 10 every 200 K, or 20 h in this case. Under what circumstances, if any, a dust-laden plume can expand into a nebular gas cloud at rates corresponding to these rates of pressure decline is not known.

5. CONCLUSIONS

Sodium saturation of the vapor coexisting with chondrules at near-liquidus temperatures requires extreme condi-

tions of dust enrichment and total pressure that have not been produced by dynamical models of the solar nebula. If CI matter is devolatilized and equilibrated in a mixture of its evaporation products with its residual nebular gas under these conditions, the resulting objects will have mineralogical and chemical compositions like those of Type II chondrules at dust enrichments as low as 400×. Ordinary chondrite-like matter processed in the same way yields objects with the properties of Type I chondrules at dust enrichments as high as 7000×. Whether the physico-chemical conditions, including total pressure, dust enrichment, peak temperature and cooling rate, required by this model can be attained in impact-generated plumes in the early solar system awaits detailed modeling.

ACKNOWLEDGMENTS

We thank F.J. Ciesla, N. Dauphas, M. Ghiorso, R. Hewins and S.B. Simon for helpful discussions, and three anonymous reviewers for comments that led to improvements in the paper. This research was supported by funds from NASA Grants NNX08AE06G and NNX13AE73G.

REFERENCES

Alexander C. M. O'D. and Ebel D. S. (2012) Questions, questions: Can the contradictions between the petrologic, isotopic, thermodynamic, and astrophysical constraints on chondrule formation be resolved? *Meteorit. Planet Sci.* **47**, 1–19.

Alexander C. M. O'D., Grossman J. N., Ebel D. S. and Ciesla F. J. (2008) The formation conditions of chondrules and chondrites. *Science* **320**, 1617–1619.

Anders E. and Grevesse N. (1989) Abundances of the elements: Meteoritic and solar. *Geochim. Cosmochim. Acta* **53**, 197–214.

Cassen P. (2001) Nebular thermal evolution and the properties of primitive planetary materials. *Meteorit. Planet. Sci.* **36**, 671–700.

Ciesla F. J. and Cuzzi J. N. (2006) The evolution of the water distribution in a viscous protoplanetary disc. *Icarus* **181**, 178–204.

Cuzzi J. N., Hogan R. C., Paque J. M. and Dobrovolskis A. R. (2001) Size-selective concentration of chondrules and other small particles in protoplanetary nebula turbulence. *Astrophys. J.* **546**, 496–508.

Davis A. M., Alexander C. M. O'D., Nagahara H. and Richter F. M. (2005) Evaporation and condensation during CAI and chondrule formation. In *Chondrites and the Protoplanetary Disk, ASP Conference Series 341* (eds. A. N. Krot, E. R. D. Scott and B. Reipurth). Astronomical Society of the Pacific, San Francisco, CA, pp. 432–455.

Ebel D. S. and Grossman L. (2000) Condensation in dust-enriched systems. *Geochim. Cosmochim. Acta* **64**, 339–366.

Fedkin A. V., Grossman L., Ciesla F. J. and Simon S. B. (2012) Mineralogical and isotopic constraints on chondrule formation from shock wave thermal histories. *Geochim. Cosmochim. Acta* **87**, 81–116.

Ghiorso M. S. and Sack R. O. (1995) Chemical mass transfer in magmatic processes IV. A revised and internally consistent thermodynamic model for the interpolation and extrapolation of liquid-solid equilibria in magmatic systems at elevated temperatures and pressures. *Contrib. Mineral. Petrol.* **119**, 197–212.

Grossman L., Fedkin A. V. and Simon S. B. (2012) Formation of the first oxidized iron in the solar system. *Meteorit. Planet. Sci.* **47**, 2160–2169.

Hashimoto A. (1983) Evaporation metamorphism in the early solar nebula-evaporation experiments on the melt FeO–MgO–SiO_2–CaO–Al_2O_3 and chemical fractionations in primitive materials. *Geochem. J.* **17**, 111–145.

Hewins R. H. and Radomsky P. M. (1990) Temperature conditions for chondrule formation. *Meteoritics* **25**, 309–318.

Hewins R. H., Zanda B. and Bendersky C. (2012) Evaporation and recondensation of sodium in Semarkona Type II chondrules. *Geochim. Cosmochim. Acta* **78**, 1–17.

Hezel D. C. and Palme H. (2010) The chemical relationship between chondrules and matrix and the chondrule matrix complementarity. *Earth Planet. Sci. Lett.* **294**, 85–93.

Huss G. R., Alexander C. M. O'D., Palme H., Bland P. A. and Wasson J. T. (2005) Genetic relationships between chondrules, fine-grained rims, and interchondrule matrix. In *Chondrites and the Protoplanetary Disk, ASP Conference Series 341* (eds. A. N. Krot, E. R. D. Scott and B. Reipurth). Astronomical Society of the Pacific, San Francisco, CA, pp. 701–731.

Jarosewich E. (1990) Chemical analyses of meteorites: A compilation of stony and iron meteorite analyses. *Meteoritics* **25**, 323–337.

Johnson C. A. and Prinz M. (1991) Chromite and olivine in type II chondrules in carbonaceous and ordinary chondrites: Implications for thermal histories and group differences. *Geochim. Cosmochim. Acta* **55**, 893–904.

Jones R. H. (1990) Petrology and mineralogy of Type II, FeO-rich chondrules in Semarkona (LL3.0): Origin by closed-system fractional crystallization, with evidence for supercooling. *Geochim. Cosmochim. Acta* **54**, 1785–1802.

Jones R. H. (1994) Petrology of FeO-poor, porphyritic pyroxene chondrules in the Semarkona chondrite. *Geochim. Cosmochim. Acta* **58**, 5325–5340.

Jones R. H. (1996) FeO-rich, porphyritic pyroxene chondrules in unequilibrated ordinary chondrites. *Geochim. Cosmochim. Acta* **60**, 3115–3138.

Jones R. H. and Scott E. R. D. (1989) Petrology and thermal history of Type IA chondrules in the Semarkona (LL3.0) chondrite. In *Proc. 19th Lunar Planet. Sci. Conf.* Lunar Planet. Inst., Houston, TX. #523–536.

Jones R. H., Grossman J. N. and Rubin A. E. (2005) Chemical, mineralogical and isotopic properties of chondrules: Clues to their origin. In *Chondrites and the Protoplanetary Disk, ASP Conference Series 341* (eds. A. N. Krot, E. R. D. Scott and B. Reipurth). Astronomical Society of the Pacific, San Francisco, CA, pp. 251–285.

Kita N. T., Nagahara H., Tachibana S., Tomomura S., Spicuzza M. J., Fournelle J. H. and Valley J. W. (2010) High precision SIMS oxygen three isotope study of chondrules in LL3 chondrites: Role of ambient gas during chondrule formation. *Geochim. Cosmochim. Acta* **74**, 6610–6635.

Lodders K. (2003) Solar system abundances and condensation temperatures of the elements. *Astrophys. J.* **591**, 1220–1247.

Richter F. M., Mendybaev R. A., Christensen J., Gaffney A. and Ebel D. S. (2009) Elemental and isotope fractionation of chondrule-like liquids by evaporation into vacuum. *Lunar Planet. Sci. XL*. #2321 (abstr.) (CD-ROM).

Richter F. M., Mendybaev R. A., Christensen J. N., Ebel D. S. and Gaffney A. (2011) Laboratory experiments bearing on the origin and evolution of olivine-rich chondrules. *Meteorit. Planet. Sci.* **46**, 1152–1178.

Ruden S. P. and Pollack J. B. (1991) The dynamical evolution of the protosolar nebula. *Astrophy. J.* **375**, 740–760.

Simon S. B., Grossman L., Podosek F. A., Zinner E. and Prombo C. A. (1994) Petrography, composition, and origin of large, chromian spinels from the Murchison meteorite. *Geochim. Cosmochim. Acta* **58**, 1313–1334.

Tachibana S., Nagahara H., Mostefaoui S. and Kita N. T. (2003) Correlation between relative ages inferred from ^{26}Al and bulk compositions of ferromagnesian chondrules in least equilibrated ordinary chondrites. *Meteorit. Planet. Sci.* **38**, 939–962.

Tachibana S., Nagahara H., Ozawa K., Ikeda Y., Nomura R., Tatsumi K. and Joh Y. (2011) Kinetic condensation and evaporation of metallic iron and implications for metallic iron dust formation. *Astrophys. J.* **736**, 1–8.

Wang J., Davis A. M., Clayton R. N., Mayeda T. K. and Hashimoto A. (2001) Chemical and isotopic fractionation during the evaporation of the $FeO–MgO–SiO_2–CaO–Al_2O_3–TiO_2$-rare earth element melt system. *Geochim. Cosmochim. Acta* **65**, 479–494.

Zhang Y., Ni H. and Chen Y. (2010) Diffusion data in silicate melts. In *Diffusion in Minerals and Melts, Reviews in Mineralogy and Geochemistry*, vol. 72 (eds. Y. Zhang and D. J. Cherniak). Mineralogical Society of America, Chantilly, VA, pp. 311–408.

Associate editor: Alexander N. Krot